Clim Dyn (2012) 39:1073–1092
DOI 10.1007/s00382-011-1147-5

Glacial-interglacial water cycle, global monsoon and atmospheric methane changes

Zhengtang Guo · Xin Zhou · Haibin Wu

Received: 1 May 2011 / Accepted: 12 July 2011 / Published online: 29 July 2011

Abstract The causes of atmospheric methane (CH_4) changes are still a major contention, in particular with regards to the relative contributions of glacial-interglacial cycles, monsoons in both hemispheres and the late Holocene human intervention. Here, we explore the CH_4 signals in the Antarctic EPICA Dome C and Vostok ice records using the methods of timeseries analyses and correlate them with insolation and geological records to address these issues. The results parse out three distinct groups of CH_4 signals attributable to different drivers. The first group ($\sim$80% variance), well tracking the marine $\delta^{18}O$ record, is attributable to glacial-interglacial modulation on the global water cycle with the effects shared by wetlands at all latitudes, from monsoonal and non-monsoonal regions in both hemispheres. The second group ($\sim$15% variance), centered at the $\sim$10-kyr semi-precession frequency, is linkable with insolation-driven tropical monsoon changes in both hemispheres. The third group ($\sim$5% variance), marked by millennial frequencies, is seemingly related with the combined effect of ice-volume and bi-hemispheric insolation changes at the precession bands. These results indicate that bi-hemispheric monsoon changes have been a constant driver of atmospheric CH_4. This mechanism also partially explains the Holocene CH_4 reversal since $\sim$5 kyr BP besides the human intervention. In the light of these results, we propose that global monsoon can be regarded as a system consisting of two main integrated components, one primarily driven by the oscillations of Inter-Tropical Convergence Zone (ITCZ) in response to the low-latitude summer insolation changes, anti-phase between the two hemispheres (i.e. the ITCZ monsoon component); and another modulated by the glacial-interglacial cycles, mostly synchronous at the global scale (i.e. the glacial-interglacial monsoon component). Although atmospheric CH_4 record integrates all wetland processes, including significant non-monsoonal contributions, it is the only and probably the best proxy available to reflect the past changes of global monsoon. However, the utility of CH_4 as a proxy of monsoon changes at any specific location is compromised by its bi-hemispheric nature.

Keywords Pleistocene · Greenhouse gases · Loess · Global monsoon

This paper is a contribution to the special issue on Global Monsoon Climate, a product of the Global Monsoon Working Group of the Past Global Changes (PAGES) project, coordinated by Pinxian Wang, Bin Wang, and Thorsten Kiefer.

Z. Guo (✉) · X. Zhou · H. Wu
Key Laboratory of Cenozoic Geology and Environment, Institute of Geology and Geophysics, Chinese Academy of Sciences, 19, Bei Tu Cheng Xi Road, Chaoyang District, P.O. Box 9825, Beijing 100029, China
e-mail: ztguo@mail.iggcas.ac.cn

X. Zhou
School of Earth and Space Sciences & Institute of Polar Environment, University of Science and Technology of China, Hefei 230026, China

1 Introduction

Methane (CH_4) is one of the greenhouse gases and directly affects atmospheric temperature through absorbing long wave radiation emitted from the Earth's surface (Wahlen 1993). Its effect is thought to have contributed $\sim$20% to the global warming since pre-industrial times (Karl et al. 2008) and would have also affected the climate system since much early geological history (Beerling et al. 2009). Measurements of atmospheric CH_4 started only in 1950s

(Hutchinson 1954) but ice records from Antarctica extended the CH_4 history to ~800 ka ago (Petit et al. 1999; Spahni et al. 2005; Loulergue et al. 2008).

The dominant sources of atmospheric CH_4 are terrestrial, such as wetlands, tundra, soils (Wahlen 1993), terrestrial plants under aerobic conditions (Keppler et al. 2006), subglacial environments (Wadham et al. 2008), wild and domestic ruminant animals (Crutzen et al. 1986), volatile organic compound sources (Kaplan et al. 2006) and biomass burning (Quay et al. 1991). Wetlands in boreal regions and between the tropics are the largest natural sources today while other wetlands are minor in proportion (Fig. 1). Their CH_4 emissions are approximately shared ~40% boreal and ~60% tropics (Aselmann and Crutzen 1989; Cao et al. 1996; Lehner and Doll 2004).

At the orbital scale, CH_4 is suggested to be sensitive to monsoon changes in the Northern Hemisphere (Ruddiman and Raymo 2003; Ziegler et al. 2010). Because tropical monsoons are thought to be primarily driven by low latitude summer insolation (Kutzbach 1981) that is marked by strong precession signals, the paradigm was used to date marine and ice records (Ruddiman and Raymo 2003). The likely in-phase changes between CH_4 and magnetic susceptibility in the China loess, particularly since 420 ka ago, is thought to support a dominant contribution of monsoon-related processes to the CH_4 variability at precession periodicities (Loulergue et al. 2008), although loess magnetic susceptibility also bears strong glacial-interglacial signals (Kukla 1987).

It was alternatively suggested that precession induced changes in northern hemispheric monsoons and associated shifts of ITCZ only play a second order role in CH_4 emission (Landais et al. 2010), as CH_4 visually tracks the glacial-interglacial cycles (Fig. 2), with much higher

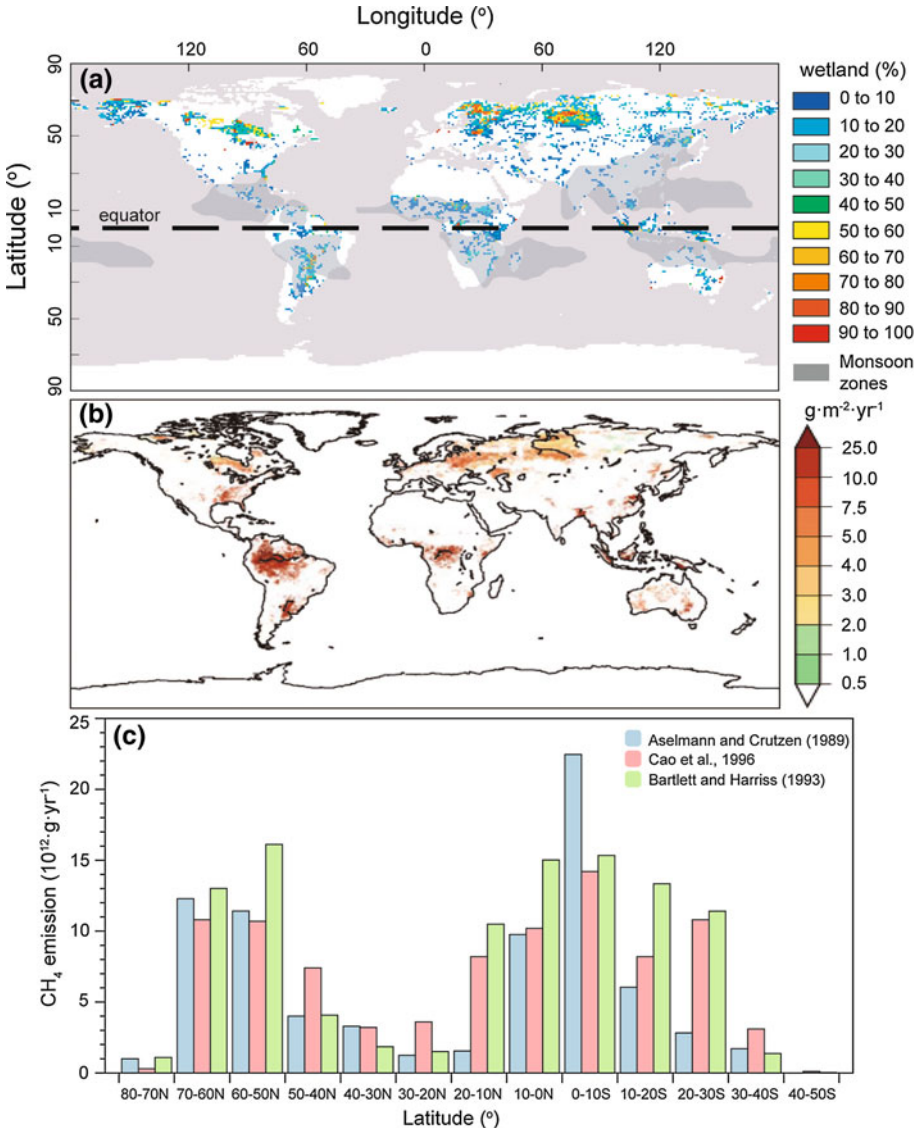

Fig. 1 Modern distributions of global wetlands, monsoon zones and CH_4 emissions. **a** Distribution of modern wetlands (Matthews and Fung 1987) and monsoon domains (*after* Wang and Ding 2008). **b** Potential natural wetlands and CH_4 emission simulated for the present (Kaplan 2002). **c** Estimates of latitudinal distribution of modern CH_4 emissions (Aselmann and Crutzen 1989; Bartlett and Harriss 1993; Cao et al. 1996)

concentrations during interglacials where boreal wetland sources are active (Schmidt et al. 2004; Landais et al. 2010). This view is likely supported by the low correlation coefficient when matching CH_4 and precession peaks (Landais et al. 2010), and by the strong 100 and 40-ka CH_4 periodicities (Loulergue et al. 2008) that are rather weak in the low-latitude insolation changes (Berger 1978), but characteristic of the glacial-interglacial cycles (Lisiecki and Raymo 2005). These may suggest that climate and hydrology changes in high latitudes have a strong role (Landais et al. 2010).

Recent correlations (Guo et al. 2009) between the China loess and Antarctic ice records raise new questions relative to the CH_4 drivers. During marine isotope stage 13 (MIS-13, ~500 ka ago), CH_4 represents the lowest interglacial values of the past 800 ka (Loulergue et al. 2008). This cannot be explained by either boreal wetlands or northern hemispheric monsoons (Guo et al. 2009), because the northern monsoons were extremely strong during this interglacial (Rossignol-Strick et al. 1998; Guo et al. 2000; Bassinot et al. 1994) (Fig. 2a), and Greenland ice-sheets substantially retreated (de Vernal and Hillaire-Marcel 2008), both would have favored CH_4 emissions.

Contentions also persist in interpreting the Holocene CH_4 changes, with an additional driver of human intervention. CH_4 decreased during the first half of the Holocene, but then reversed direction and began to increase ~5,000 years ago. This reversal and subsequent increase have been variously attributed to natural (Schmidt et al. 2004) and anthropogenic (Ruddiman 2003; Ruddiman and Thomson 2001) factors. A potential role of the Southern Hemisphere climate was also invoked (Brook 2009), as is recently supported by CH_4 modelling for the Holocene (Singarayer et al. 2011).

Summarizing from these views, it becomes clear that past CH_4 changes mainly consist of a mixture of the signals from boreal wetlands, and from both southern and northern monsoon regions, but several fundamental questions remain to be addressed. First, the relative contributions and variance of these main sources in the past are still

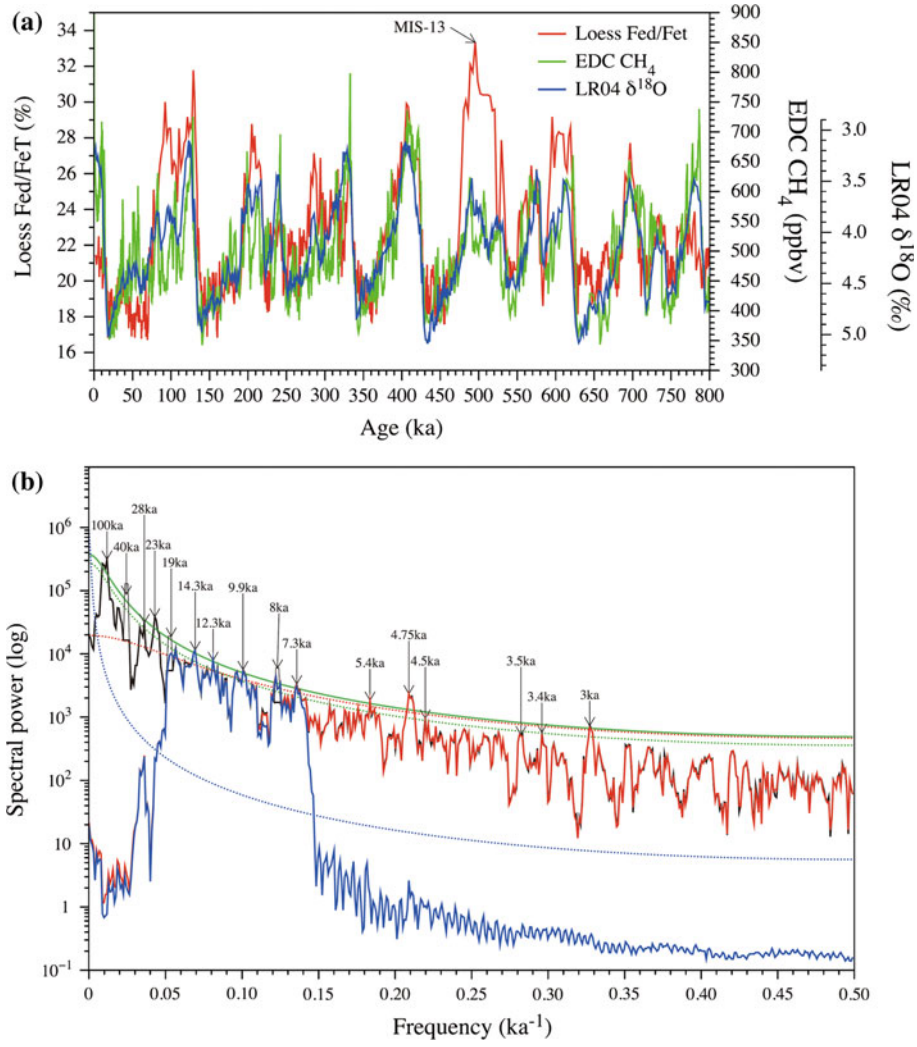

Fig. 2 Comparison of atmospheric CH_4, global ice-volume and East Asian monsoon changes in the past 800 ka. **a** EDC CH_4 (Loulergue et al. 2008), LR04 marine $\delta^{18}O$ (Lisiecki and Raymo 2005) and Chinese loess weathering (Fed/Fet) (Guo et al. 2000) records. **b** Multi-taper spectrum (MTM) of EDC CH_4 record (*black line*, with *green continuous* and *dotted lines* indicating 99 and 95% confidence levels, respectively). MTM spectra of EDC CH_4-G2 (*red continuous line*, with *red dotted line* showing 99% confidence level) and EDC CH_4-G2a (*blue continuous line*, with *blue dotted line* indicating 99% confidence level) are also shown for comparison. MTM analyses are performed using the EDC3 timescale (Parrenin et al. 2007)

controversial. The glacial-interglacial signals in the CH_4 records have mostly been linked with boreal wetlands (Landais et al. 2010) while the contributions of monsoon-related wetlands to these signals are not yet clear. Second, distinguishing the relative contributions of northern and southern hemispheric monsoons is critical for understanding the CH_4 dynamics and for evaluating the human impacts in the late Holocene. Another major challenge is to understand why CH_4 changes by up to half its glacial-interglacial range many times during the glacial periods (Wolff and Spahni 2007; Wolff 2011). Because atmospheric CH_4 changes are frequently linked with monsoon climates, all of these would provide helpful insights for addressing the paleo-monsoon dynamics, particularly if all regional monsoons are viewed as a integrated system of global scale, i.e. the global monsoon (Wang 2009). One of the efficient ways for addressing these issues is to make the mixed CH_4 signals decomposed, to compare them with representative geological records, and to interpret their causal links with climate-driven wetland processes, as are the main aims of this study.

In Sect. 2, we firstly decompose the 800-ka EPICA Dome C (EDC) (Loulergue et al. 2008) and the 420-ka Vostok (Petit et al. 1999) CH_4 records using Singular Spectrum Analysis (SSA) (Ghil et al. 2002). The decomposed principle components (PCs) are then reconstructed into different fractions based on the main known/potential CH_4 drivers in order to address their links and to evaluate their relative variances. In Sect. 3, the reconstructed CH_4 fractions are compared with relevant marine and terrestrial records and with insolation to testify the above causal links, discuss the underlying climate-wetland processes, and explore the relationships between CH_4 cycle and global monsoon. In the light of these results, the human and natural interventions on the Holocene CH_4 trends, a contentious issue of Paleoclimatology, are also discussed in Sect. 4.

2 Atmospheric methane signals

The EDC ice core contains a record of atmospheric CH_4 for the past 800 ka with the average time resolution of $\sim$380 years and analytical uncertainty of $\sim$10 ppbv (Loulergue et al. 2008). The Vostok CH_4 record covers the past 420 ka with the average time resolution of $\sim$900 years and analitical uncertainty of $\sim$20 ppbv (Petit et al. 1999). The EDC3 chronology (Parrenin et al. 2007), with an estimated uncertainty of 3–6 ka, is used in this study for both EDC and Vostok records. The EDC3 gas age for Vostok is from Luthi et al. (2008). Detailed information about the CH_4 data and their chronology are given in the origianl references (Petit et al. 1999; Parrenin et al. 2007; Loulergue et al. 2008).

We perform a spectral analysis (Fig. 2b) on the 800-ka EDC CH_4 record (Loulergue et al. 2008). The results show clear periods at $\sim$100, $\sim$40, $\sim$23, $\sim$19, $\sim$14.3, $\sim$9.9, $\sim$8–7.3, $\sim$5.4, $\sim$4.75 and $\sim$3 ka over the 99% confidence level. Part of these peaks was already reported (Loulergue et al. 2008). Periods at $\sim$28, $\sim$12.3, $\sim$4.5 and $\sim$3.4 ka over the 95% confidence level are also detected. Analysis on the Vostok CH_4 record yields essentially similar results, but the $\sim$3-ka peak at EDC is not detectable at Vostok.

Among the available tools for timeseries decomposition, SSA is a nonparametric method that allows the decomposition and reconstruction of signals from a timeseries in overcoming the problems of finite sample length and noisiness. One of the advantages of SSA decomposition is the use of a data adaptive basis set (Ghil et al. 2002), instead of fitting an assumed model. The method allows decomposing a timeseries into different components with the variance evaluated, and has widely been used in paleoclimate studies (Gamiz-Fortis et al. 2002; Cosford et al. 2008; Pisias et al. 2010) for signal explorations.

We use a window length of 80 ($M = 80$) for the EDC CH_4 record following the suggestion that the window length should be less than about 1/5 of the point number in the timeseries (Vautard et al. 1992) as CH_4 data are equally spaced at 1-ka intervals before the analyses. Burg covariance estimation (Penland et al. 1991) and Heuristic significant tests (Ghil et al. 2002) are used for the SSA decomposition. Eighty SSA principal components (PCs) are thus obtained for EDC. Their relative power, indicative of the variance of each component, is ranked in Fig. 3b. Similar analyses are performed on the Vostok CH_4 record with 41 PCs decomposed ($M = 41$). We assume that all the PCs represent true CH_4 signals and none of them is removed in the subsequent analyses.

Among the known/potential drivers of CH_4 invoked in earlier studies, glacial-interglacial changes, as indicated by the marine $\delta^{18}O$ record (Lisiecki and Raymo 2005), are marked by strong $\sim$100 and $\sim$40-ka periodicities while low latitude summer insolation is primarily driven by precession, dominated by the 23 and 19-ka signals (Berger 1978). The strong $\sim$100 and $\sim$40-ka periods in the CH_4 records confirm the link with the glacial-interglacial cycles (Landais et al. 2010; Loulergue et al. 2008), as is even seen through visual examination on the CH_4 and marine $\delta^{18}O$ records (Fig. 2a).

Given that glacial-interglacial cycles certainly affected atmospheric CH_4 despite of the contentions about their relative contributions, we firstly use part of the SSA PCs to reconstruct the CH_4 signals until the reconstruction matching, at farthest, the full marine $\delta^{18}O$ record (Lisiecki and Raymo 2005), with the aim at evaluating the CH_4 variance linkable with the glacial-interglacial cycles. The

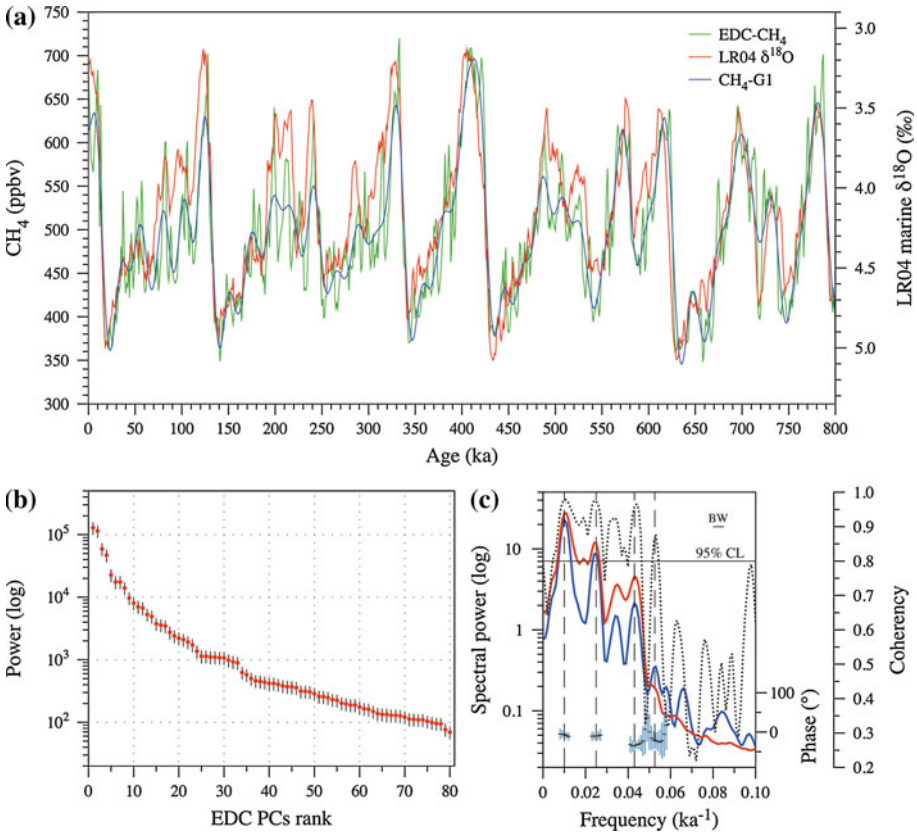

Fig. 3 Reconstructed CH_4-G1 for EDC using Singular Spectrum Analysis (*SSA*) (Ghil et al. 2002) and comparison with marine $\delta^{18}O$ record. EDC CH_4 (Loulergue et al. 2008) is decomposed into 80 PCs with CH_4-G1 reconstructed from PC1-8, CH_4-G2 from PC9-80, CH_4-G2a from PC9-23 and CH_4-G2b from PC24-80. **a** Variations of CH_4-G1, original EDC CH_4 data (Loulergue et al. 2008) and LR04 marine $\delta^{18}O$ (Lisiecki and Raymo 2005). **b** Ranks of powers for the 80 SSA principal components (*PCs*) of EDC CH_4. **c** Blackman–Tukey spectra of CH_4-G1 (*red*) and LR04 $\delta^{18}O$ (*blue*), coherency (*black dotted line*) and phase (*black tick* with *light blue error bar*). *Vertical discontinuous lines* indicate the 100, 40, 23 and 19-ka orbital bands. CH_4-G1 lags LR04 $\delta^{18}O$ by 6° at the ~100-ka band, 10° at the ~40-ka band, 35° at the ~23-ka band and 20° at the ~19-ka band

reconstruction (CH_4-G1) using PC1-8 of EDC best matches marine $\delta^{18}O$ with a total variance up to ~80% (Fig. 3a). The number of PCs used are rather strict because adding PC9 into CH_4-G1 over-accentuates the ~20-ka signals in comparison with those in the marine $\delta^{18}O$ record. Linear correlation between CH_4-G1 and marine $\delta^{18}O$ (Lisiecki and Raymo 2005) yields a correlation coefficient (R^2) of 0.77. Analyses on the Vostok CH_4 record yield essentially similar results (Fig. 4) with CH_4-G1 reconstructed from PC1-4. The long-term variations of CH_4 are obviously dominated by the CH_4-G1 fraction. Cross-spectral analyses reveal strong coherencies between EDC CH_4-G1 and marine $\delta^{18}O$ at the 100-ka eccentricity, 40-ka obliquity, 23 and 19-ka precession bands (Fig. 3c), supporting again the link between CH_4-G1 and the glacial-interglacial cycles.

After removing CH_4-G1 from the initial CH_4 records, the remained components, referred to as CH_4-G2, are compared with the original data (Fig. 4). Although this part contains millennial CH_4 signals (Fig. 2b), the dominant ~20 and ~10-ka periodicities are visually definable (Fig. 4). Examinations on individual SSA PC reveal that millennial CH_4 signals (Figs. 4, 6a) mainly reside in PC24-80 (Fig. 3b) for EDC. Because this part of the signals (Fig. 6a) is not directly linkable to orbital parameters, it is temporarily removed apart (CH_4-G2b) in order to better examine the orbital scale changes. This step yields CH_4-G2a shown in Figs. 4 and 5. They consist of PC9-23 for

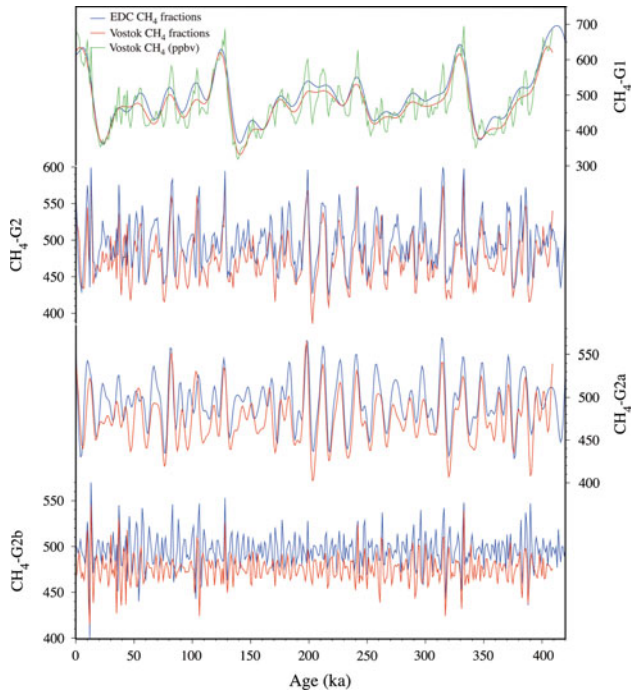

Fig. 4 SSA reconstructed CH_4 signals for Vostok and comparison with EDC results. Vostok CH_4 (Petit et al. 1999) versus EDC3 timescale (gas age from Luthi et al. 2008) is decomposed into 41 PCs with G1 reconstructed from PC1-4, G2 from PC5-41, G2a from PC5-12 and G2b from PC13-41. *Green line* in the *top* panel shows original Vostok CH_4 data for comparison

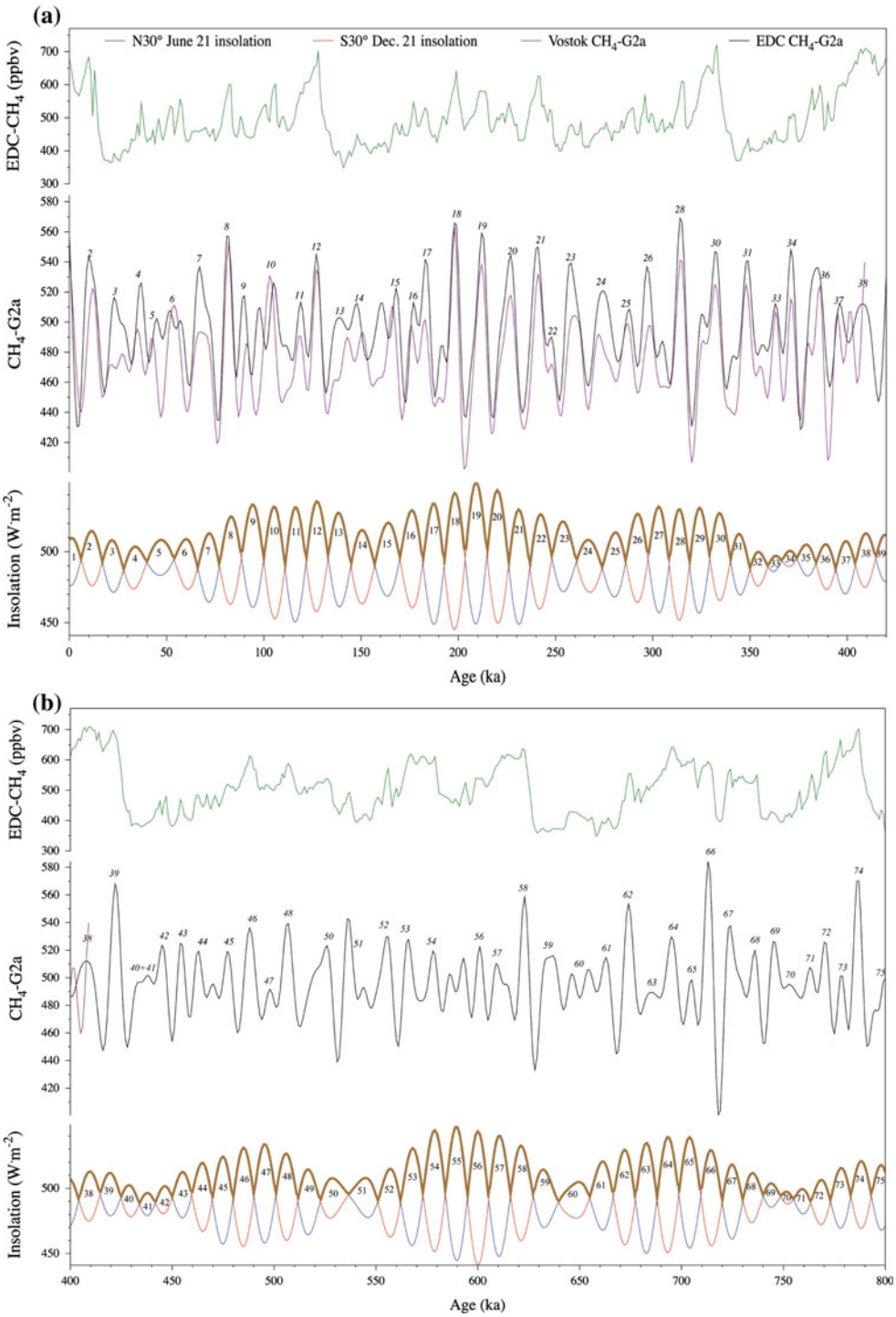

Fig. 5 Peak-to-peak match between CH_4-G2a with bi-hemispheric insolation (BHI, defined as the time evolution of maximum N30° (June 21) and S30° (Dec. 21) summer insolation values (Berger 1978)). **a** Matching pattern for the interval 0–420 ka BP. **b** Matching pattern for the interval 400–800 ka BP. Original EDC CH_4 data (Loulergue et al. 2008) are shown for comparison. Correspondent *numbers* show the proposed peak-to-peak match between BHI and CH4-G2a. *Thick brown lines* indicate BHI

EDC CH_4 with a total variance of ~15%. The boundary between CH_4-G2a and CH_4-G2b is not as strict as for that between CH_4-G1 and CH_4-G2: adding or removing a few PCs does not significantly affect the basic spectral features and variance estimates for CH_4-G2a and CH_4-G2b because PCs ranked beyond 20 have quite small (<0.41%) variances (Fig. 3b). The three CH_4 fractions from Vostok (Petit et al. 1999) are essentially similar to the EDC ones (Figs. 4, 5), with CH_4-G1 constructed from PC1-4, CH_4-G2a from PC5-12 and CH_4-G2b from PC13-41.

Although low latitude summer insolation in the Northern Hemisphere is among the important CH_4 drivers (Ruddiman and Raymo 2003), this factor alone is clearly insufficient to explain CH_4-G2a because insolation dominantly varies at the ~20-ka frequency while CH_4-G2a show much more maxima occurring roughly every 10 ka

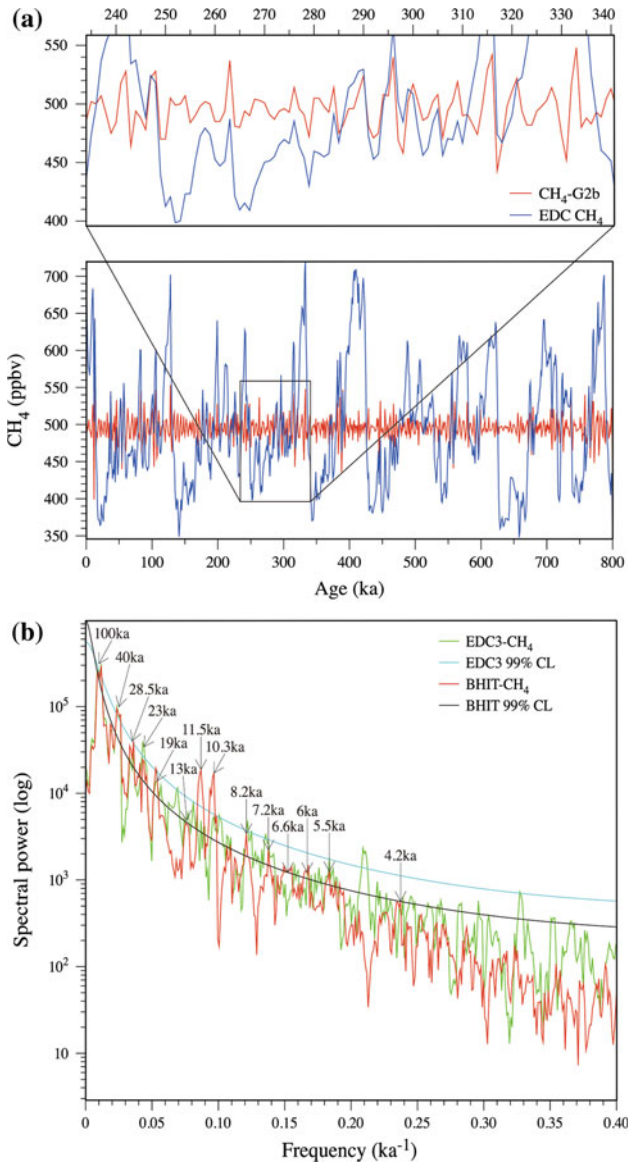

Fig. 6 EDC CH_4-G2b and spectral features after bi-hemispheric insolation tuning (*BHIT*). **a** EDC CH_4-G2b compared with original EDC data (Loulergue et al. 2008). **b** Comparison of MTM spectra between EDC CH_4 plotted versus EDC3 chronology and that plotted versus the BHIT timescale through matching CH_4-G2a and BHI following the peak-to-peak pattern in Fig. 5. Periods over the 99% confidence level are labeled. Spectral peaks at the orbital bands over the 99% confidence level are largely enhanced for BHIT-CH_4

(Fig. 5), approximately at the semi-precession frequency. This is also clear in the MTM-spectrum of CH_4-G2a (Fig. 2b) marked by a *plateau* centered at the ~10-ka frequency with several sub-order peaks, including clear ~20 and ~10-ka ones.

These may suggest two possibilities: (1) except the ~20 and ~10-ka signals directly linkable with orbital forcing, the other sub-order peaks on the spectral *plateau* of CH_4-G2a (Fig. 2b) also represent true CH_4 cycles linked with some unknown drivers; or (2) the other sub-order peaks are partly caused by the ~3–6 ka uncertainty of the EDC3 timescale (Parrenin et al. 2007).

To clarify these possibilities, we firstly compare CH_4-G2a maxima with low latitude summer insolation of the Northern Hemisphere (Fig. 5), one of the key drivers of monsoons and CH_4. Within the accuracy of the EDC3 timescale, about half of the CH_4-G2a peaks roughly match the northern insolation maxima, and the other half mostly locates between the northern insolation peaks. However, these peaks approximately match the maxima of low latitude summer insolation in the Southern Hemisphere (Fig. 5). Some CH_4-G2a peaks show slight dislocations from the insolation maxima, but mostly within a few kiloyears. Although there is a kind of uncertainty in matching a small part of the peaks, the overall correlativity between CH_4-G2a and insolation is unambiguous (Fig. 5).

As a further check of this observation, we tune CH_4-G2a onto the bi-hemispheric insolation (BHI, defined as the time evolution of maximum N30° and S30° summer insolation values) using the peak-to-peak matching pattern in Fig. 5. This slightly changes the EDC3 timescale but mostly within its estimated uncertainty of 3–6 ka (Parrenin et al. 2007). The tuning not only accentuates the semi-precession frequencies of the CH_4 timeseries, but also substantially enhances the spectral power over the 99% confidence level at all the main orbital bands (Fig. 6b), i.e. the ~100, 40, 23 and 19 ka. These attest to an increased accuracy of the timescale, and hence strongly support the link between CH_4-G2a and the bi-hemispheric insolation (Fig. 5). The Mt Berlin eruption at EDC-1265.1 m depth, the only independent isotopic age control of EDC3 prior to the Holocene (Parrenin et al. 2007), is closer to his Ar/Ar age (92.5 ± 2 ka) (gas age 87.7 ka vs. 85.7 ka in EDC3), and the B/M boundary age remains unchanged after the tuning.

The CH_4-G2b fraction (Fig. 6a), dominated by millennial signals (Fig. 2b), represents a total variance of ~5% in average. After the bi-hemispheric insolation tuning (BHIT) of CH_4-G2a, these millennial oscillations at EDC center at ~8.2, 7.2, 6.6, 6, 5.5 and 4.2 ka (Fig. 6b), but the ~3-ka peak (Fig. 2b) disappeared. The peak at ~28 ka is also largely reinforced (Fig. 6b).

Our analyses thus parse out three distinct CH_4 fractions. The largest one (CH_4-G1, ~80% variance) well tracks marine $\delta^{18}O$ record (Fig. 3a). After removing CH_4-G1, the remained fraction (CH_4-G2, ~20% variance) mainly contains precession, semi-precession and millennial CH_4 signals. CH_4-G2 can be further parsed into CH_4-G2a (~15% variance) closely matching the low latitude summer insolation in both Southern and Northern Hemispheres (Figs. 4, 5), and CH_4-G2b (~5% variance) marked by millennial oscillations (Fig. 6a). These offer the possibility

to correlate different CH_4 fractions with relevant geological records for better understanding the underlying climate-wetland processes.

3 Linking methane signals with geological records

3.1 Glacial-interglacial controls

The CH_4-G1 fraction with a variance of ~80% is thus causally linkable with the glacial-interglacial cycles (Figs. 3a, 4). CH_4-G1 slightly lags marine $\delta^{18}O$ at all the main orbital frequencies (Fig. 3c), supporting again that the glacial-interglacial cycles are a primary driver of atmospheric CH_4 changes. This link is also supported by relevant geological records at the global scale, and by the climate-wetland processes mostly congruent with climate modeling, as are discussed below.

Although glacial-interglacial cycles affect the climate system through many mechanisms, including the changes in the ocean and atmospheric circulations, their modulation on the global water cycle should be the dominant pathway in introducing the signals into the CH_4 history, as wetlands are the main sources of CH_4. Several mechanisms would have synchronously operated at the global scale, but with a common feature that CH_4 emission is favored when ice-volume is smaller.

A first process is the glacial-interglacial control on high latitude wetlands (Chappellaz et al. 1997b; Petit et al. 1999; Wolff and Spahni 2007; Loulergue et al. 2008). Under the present interglacial conditions, global wetlands are approximately shared ~50–60% boreal and 40–50% tropics (Lehner and Doll 2004) (Fig. 1a). Their CH_4 emissions represent ~40 and 60% of the global CH_4 emission (Cao et al. 1996; Lehner and Doll 2004), respectively (Fig. 1c). Emissions from other wetlands are minor in proportion (Fig. 1).

At the glacial-interglacial scale, the more extended periglacial wetlands due to ice-sheet retreat and the higher temperature in the interglacials favor CH_4 emission, which is essentially shut down under glacial conditions (Fischer et al. 2008). This suggests a boreal CH_4 contribution generally smaller than ~40% following the glacial-interglacial cycles if its modern proportion is assumed for the past interglacial periods.

Moisture availability and temperature changes at the global scale would have also played an important role. Global atmospheric water contents during the interglacials should be much higher than for the glacials because atmospheric water-holding capacity increases roughly exponentially with temperature (Trenberth et al. 2003; Min et al. 2011). Also, interglacial (warmer)/glacial (cooler) oceans naturally provide more/less moisture to the continents, leading to expanded/reduced wetlands (CH_4 emissions). Higher interglacial continental temperature also favors CH_4 emissions as groundwater table and temperature have strong effects on CH_4 emissions today (Walter and Heimann 2000) despite of the possibly different order of magnitude for the past. Continents at all latitudes in both hemispheres, including the monsoonal and non-monsoonal zones, must have shared these effects.

This interpretation is strongly supported by the synchronous glacial-interglacial patterns in the eolian dust fluxes in Asia (Guo et al. 2009), North Pacific (Hovan et al. 1989), tropical Pacific (Winckler et al. 2008), North Africa (Clemens et al. 1991, 1996; deMenocal 1995) and Antarctica (Lambert et al. 2008) (Fig. 7a), a proxy commonly considered indicative of continental humidity in the dust source regions although the significance of Antarctic dust record is somewhat different (Lambert et al. 2008).

Another important process would be the glacial-interglacial influences on monsoon circulations, among which the East Asian and Australian monsoon are worthy particular attentions. The history of East Asian monsoon recorded in the loess-soil sequences in China strongly supports this interpretation, as all proxies relative to the summer monsoon (Guo et al. 1998, 2000, 2009) display clear oscillations correlative with the glacial-interglacial cycles and atmospheric CH_4 trends (Fig. 2a).

The East Asian monsoon may be the strongest monsoon. Its direct influences are not limited within the tropical zones with ITCZ oscillations, but also determine the rainfall in the Asian interior at least north to 40°N (Wang et al. 2005; Wang 2006). This particular feature is attributable to several mechanisms.

East Asian monsoon is sensitive to the land-sea thermal contrasts between the tropical Pacific and Indian Oceans and Asian continent (Halley 1986; Ding et al. 2004; Lestari and Iwasaki 2006). Oceanographic data (de Garidel-Thoron et al. 2005; Li et al. 2008; Mohtadi et al. 2010) effectively show prominent changes in the tropical sea surface temperatures (SST) following the glacial-interglacial cycles. These must have affected the land-sea thermal contrasts, and hence, the strength of East Asian monsoon besides summer insolation changes.

The surface conditions of Tibetan Plateau also have strong impacts on the strength of East Asian monsoon (Yasunari 2007; Souma and Wang 2010). Geological records (Chen et al. 1999) shows that Tibetan Plateau was significantly warmed during the interglacials, but mostly frozen during the glacials. These must have strongly modulated the monsoon circulation and CH_4 emissions from the elevated wetlands, and consequently introduced the glacial-interglacial signals into the East Asian monsoon and CH_4 records.

Climate models (Jiang and Lang 2010) suggest that glacial-interglacial sea-level changes have also strongly effects in the monsoon rainfall in East Asia. During the Last Glacial Maximum, sea-level drop led to a retreat of the shoreline ~1,000 km farer than for the present-day (Wang et al. 2005). Consequently, the East Asian continent would have received much less monsoon rainfall, disfavoring wetlands and CH_4 emissions.

Another factor would be the Asian winter monsoon that is strongly controlled by the northern high latitude climates (Ding et al. 1995; Guo et al. 2004), i.e. the glacial-interglacial cycles. The reinforced winter monsoon during the glacials in response to the ice-volume increase would have led to annually shorter summer monsoon controls, and consequently, to reduced monsoon wetlands and CH_4 emissions.

The Australian monsoon also significantly differs from the tropical monsoons. Lake level changes (Magee et al. 2004) at the precession band sometimes match the southern summer insolation (Fig. 7b), as is consistent with the model output (Wyrwoll and Valdes 2003). However, lake levels were significantly higher during the interglacials than for the glacials (Magee et al. 2004) (Fig. 7b). These imply two overlapped components, one approximately in-phase with the glacial-interglacial cycles, and another corresponding to the low latitude insolation changes, roughly anti-phasing the northern monsoons at the precession band (Fig. 7b). Except the temperature effect, the clear glacial-interglacial signals in the Australian summer monsoon are also attributable to the cross-equator Asian winter monsoon that reinforces the Australian summer monsoon (Wyrwoll and Miller 2001) and to ice-induced seal-level changes (Griffiths et al. 2009).

From these lines of evidence, it is clearly emerged that East Asian and Australian monsoons consist of two main components, one primarily driven by the low latitude summer insolation, and another forced by the glacial-interglacial cycles. The first one is mainly associated with the ITCZ oscillations and anti-phase between Asia and Australia (i.e. the ITCZ monsoon component), whereas the second is synchronously forced by the glacial-interglacial cycles (i.e. the glacial-interglacial monsoon component).

These two monsoon components integrate and finally determine the monsoon rainfall, and subsequently, the wetland extents and their CH_4 emissions. The ITCZ monsoon component is more accentuated in the tropical regions while the glacial-interglacial monsoon component becomes increasingly prominent towards mid-latitudes.

In summary, the main processes introducing the glacial-interglacial signals into the CH_4 history include not only the changes of boreal wetlands, but also the glacial-interglacial influences on the global moisture availability and on the monsoon-related wetlands at various latitudes.

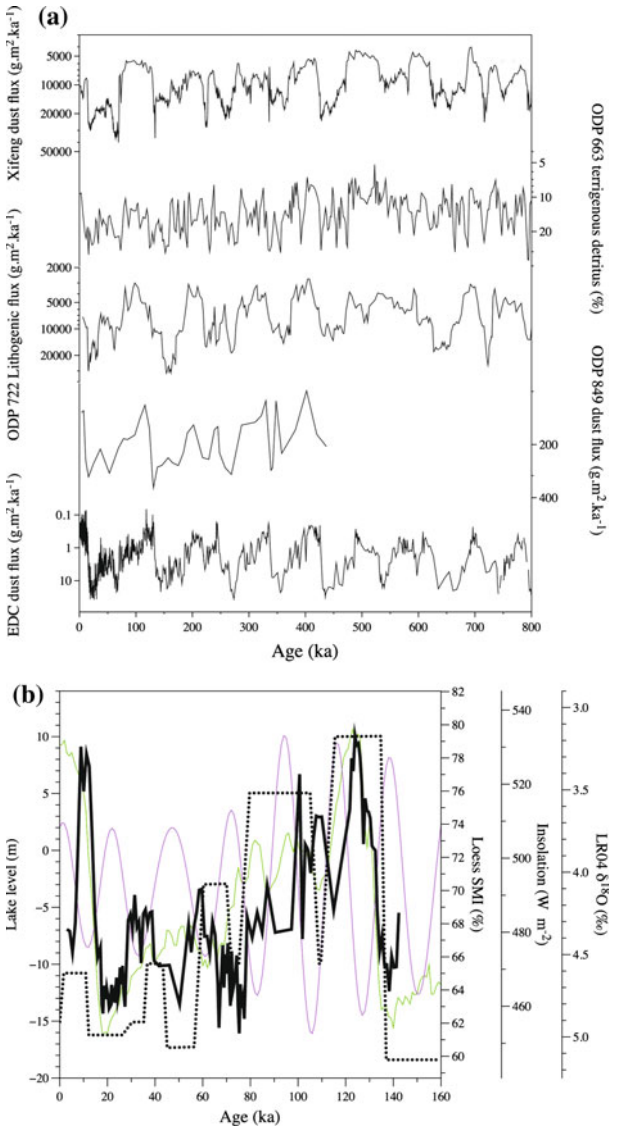

Fig. 7 Global synchronous changes of continental humidity following the glacial-interglacial cycles. **a** Eolian dust indicators of continental humidity. Lower dust flux or less terrigenous detritus reflect more humid conditions in dust source regions. Xifeng (China) data (Guo et al. 2009) are indicative for the Asian interior; Terrigenous detritus at ODP 663 (deMenocal 1995) are indicative for tropical Africa; Data from ODP 722 (Clemens et al. 1996) is indicative for tropical Arabia and Somalia; Data from east equatorial Pacific ODP 849 site (Winckler et al. 2008) are indicative for northern South America. Significance of EDC dust flux (Lambert et al. 2008) appears to be complex because of the changes in dust sources and circulations following the glacial-interglacial cycles. **b** Summer monsoon index (*SMI*, *continuous black line*) from the Weinan loess section in China (Liu et al. 1995) and monsoon induced lake level changes (*dotted black line*) of Eyre Lake in Australia (Magee et al. 2004). SMI at Weinan was derived from a chemical weathering index to reflect the strength of East Asian summer monsoon. SMI is tuned to N30° summer insolation because northern monsoons at the precession band are mostly considered in phase with insolation changes. S30° summer insolation (*fine purple line*) (Berger 1978) and LR04 marine $\delta^{18}O$ (*fine green line*) (Lisiecki and Raymo 2005) are shown for comparison

Compensation between the sources and sinks may also be affected by the glacial-interglacial cycles (Loulergue et al. 2008). Our analyses in Sect. 2 suggest that a comprehensive account of these processes would contribute ~80% to the CH_4 variability in average although the variance changed through time due to variable and complex combinations of the boundary conditions.

MIS-13 constitutes a spectacular example of this complexity (Fig. 2a). Atmospheric CH_4 at this time represents rather low interglacial values of the past 800 ka (Loulergue et al. 2008). However, geological records consistently show significantly warmer conditions for the northern high latitudes. Mountain glaciers in the Baikal region were mostly melted (Prokopenko et al. 2002). Extremely strong paleosols were developed in eastern (Markovic et al. 2009) and northern Europe (Zagwijn 1996; Vandenberghe 2000), associated with a total lack of ice-rafted debris (McManus et al. 1999) during a long interval at some North Atlantic sites. Greenland ice-sheet was substantially melted (De Vernal and Hillaire-Marcel 2008). These indicate that boreal wetlands were not dominant for the CH_4 concentrations during MIS-13 because warmer conditions and ice-sheet melt at northern high latitudes would have led to more extended boreal wetlands and increased CH_4 emissions.

The low CH_4 concentrations during MIS-13 are also strongly decoupled with the northern hemispheric monsoons. Loess records in northern China (Fig. 2a) show an extremely strong summer monsoon (Guo et al. 1998, 2009), as is also evidenced by the widely spread vermiculated soil complex in southern China (Yin and Guo 2006). The event has clear signature in South China Sea (Wang et al. 2003). An unusually strong African monsoon (Rossignol-Strick et al. 1998) at this time was also recorded by a thick Mediterranean sapropel resulting from high flooding of the Nile River. The tropical Indian Ocean was marked by low salinity during MIS-13, suggesting increased fluvial fresh water input associated with strong Indian monsoon (Bassinot et al. 1994). These suggest commonly strengthened monsoon circulations in the Northern Hemisphere that would have also increased CH_4 emissions from the northern low latitudes. The strong monsoons would even have affected the marine carbon reservoir (Wang et al. 2003). The strong MIS-13 soils in terrestrial records are sometimes interpreted as the results of longer interglacial duration, but the prominent positive $\delta^{13}C$ excursions in the world oceans indicate a climate signature instead of a time effect (Guo et al. 1998, 2009).

Marine $\delta^{18}O$ record (Lisiecki and Raymo 2005) shows that global ice volume during MIS-13 (Fig. 2a) was greater than for most of the other interglacials in the past 800 ka, but ice would have mainly stocked in Antarctica in view of the substantial melt of Greenland ice-sheets (de Vernal and Hillaire-Marcel 2008). These are consistent with the ~4°C lower temperature in Antarctica than for the Holocene (Jouzel et al. 2007), and supported by the much lower sea surface temperatures in sub-Antarctic Atlantic (Becquey and Gersonde 2003; Martínez-Garcia et al. 2009), Southeast Atlantic (McClymont et al. 2005) and Southwest Pacific (King and Howard 2000) in comparison with the other mid-Pleistocene interglacials.

Thus, geological records indicate a much cooler Southern Hemisphere versus a substantially warmed Northern Hemisphere, and hence a strong asymmetry of hemispheric climates during MIS-13 (Guo et al. 2009). This suggests that the glacial-interglacial changes do not always comply with the Milankovitch rule that emphasizes the role of summer insolation changes at northern high latitude on the global ice-volume (Milankovitch 1948). Such an asymmetrical scenario is favorable to northwards migration of ITCZ (Iriondo 2000; Markgraf et al. 2000; Cox et al. 2008) that enhances the northern monsoons, as is likely congruent with the sea surface salinity (Sepulcre et al. 2011) and terrestrial vegetation changes near the ITCZ around MIS-13 (Horikawa et al. 2010).

The lowest interglacial CH_4 values associated with the much warmer high latitudes and strong monsoons in the Northern Hemisphere need to invoke an offset by largely reduced CH_4 emissions from other regions. Although ice conditions during MIS-13 is less clear for high latitude North America due to the lack of relevant geological record, data from the mid-latitude continent show that MIS-13 was even mostly warmer than MIS-11 (Fawcett et al. 2011). It is incredible that Eurasian and North Atlantic high latitudes were exceptionally warmer while high latitude North America was cooler.

The only plausible explanation for the lowest interglacial CH_4 values during MIS-13 is the reduced emissions from the Southern Hemisphere due to the cooler climates. The related effects must have been sufficiently large to recompense the stronger CH_4 emissions of the northern monsoon and boreal wetlands. The lower SST near the tropics (De Garidel-Thoron et al. 2005; Li et al. 2008) associated with the cooler Southern Ocean would have also cooled the tropical continents, and led to less CH_4 emissions. Thus, MIS-13 provides an example that southern hemispheric climates may dominate the global CH_4 signals at the glacial-interglacial scale.

3.2 Bi-hemispheric tropical monsoons and methane changes

The CH_4-G2a fraction, with a variance of ~15%, is characterized by the lack of 100 and 40-ka periodicities (Figs. 4, 5), indicating a relative independence from the glacial-interglacial cycles. Its fluctuations, dominantly at

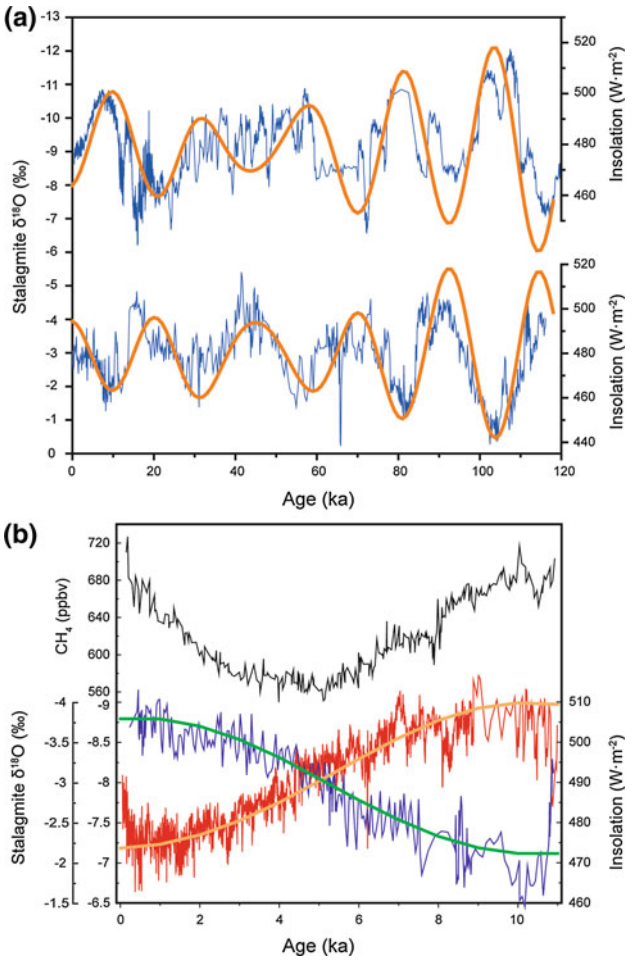

Fig. 8 Anti-phase changes of Asian and South American monsoons at the precession bands compared with the Holocene CH_4 trends. **a** Asian and South American monsoon events as indicated by stalagmite $\delta^{18}O$ records (*blue line*) from southern China (Hulu and Dongge Caves) (Wang et al. 2008) and Brazil (Caverna Botuverá) (Cruz et al. 2005). *Thick orange lines* represent summer daily insolation changes at N30° (June 21, *upper* curve) and S30° (Dec. 21, *lower* curve) (Berger 1978). **b** Comparison of the Holocene CH_4 changes (Loulergue et al. 2008) with stalagmite records and summer insolation at N30° (*orange*) and S30° (*green*) (Berger 1978). Stalagmite $\delta^{18}O$ for South America and East Asia are from Caverna Botuverá, Brazil (*blue*) (Cruz et al. 2005) and Dongge Cave, China (*red*) (Wang et al. 2005), respectively

the precession and semi-precession frequencies, are correlative with the low latitude summer insolation changes from both hemispheres (Fig. 5). In parallel with the well-known contribution of the northern tropical wetlands, this indeed justifies again the prominent contribution of tropical monsoon wetlands in the Southern Hemisphere that is previously underestimated in interpreting the past CH_4 changes.

Accounts of modern wetlands and CH_4 emissions (Fig. 1) strongly support this interpretation. Tropical wetlands currently represent ~40–50% of the global wetland surface, but more than half or two-third in the Southern Hemisphere. They contribute ~60% of the CH_4 emissions today with a southern hemispheric emission ~1.2–1.5 times (Fig. 1c) compared to the northern one (Aselmann and Crutzen 1989; Cao et al. 1996; Lehner and Doll 2004).

The reconstruction of the present natural wetlands (Fig. 1a) would underestimate the total surface of tropical wetlands, particularly for Asia and Africa, because of the conversion of natural wetlands to agriculture. Model stimulation for the present-day show much extended potential wetlands and CH_4 emissions in the tropical regions of both hemispheres (Kaplan 2002) (Fig. 1b). The southern South America (Fig. 1b) is among the largest modern CH_4 emitters (Kaplan 2002; Lehner and Doll 2004). These are also supported by the modern precipitation observations (Huffman et al. 2009) showing greater values for the southern monsoonal continents than for the northern ones. Such an emission pattern must have figured in the past.

As a fundamental difference from the East Asian and Australian monsoons, tropical monsoons are primarily associated with the seasonal oscillations of ITCZ (Wang 2006), prevailing the tropical Asia (Wang et al. 2008), North and South Africa (Kutzbach 1981), North (Poore et al. 2005) and South America (Cruz et al. 2005). Climate models suggest that the strengths of tropical monsoons are prominently driven by low latitude summer insolation changes in each of the hemispheres (Kutzbach 1981; Kutzbach and Liu 1997; Wyrwoll and Valdes 2003), as is in agreement with the geological records (Fig. 8).

High-resolution data in the Northern Hemisphere with well-constrained chronologies, from tropical South Asia (Yuan et al. 2004; Kelly et al. 2006) and East Asia (Zheng and Lei 1999; Wang et al. 2008), North Africa (Gasse 2000; Adegbie et al. 2003), and North America (Haug et al. 2001; Poore et al. 2005) consistently show that the late Pleistocene monsoon histories roughly match the northern summer insolation changes, with strong precession signals at the ~20-ka frequency. Similarly, data from South Africa (Partridge et al. 1997; Bonnefille and Chalié 2000; Barker et al. 2003) and South America (Seltzer et al. 2000; Wang et al. 2004; Cruz et al. 2005) show equally prominent signals of low latitude summer insolation of the Southern Hemisphere, but roughly anti-phasing the northern monsoon changes at the precession band (Fig. 8). Semi-precession oscillations are naturally obvious in the equatorial monsoon rainfall (Verschuren et al. 2009) due to the ITCZ oscillations in response to bi-hemispheric insolation changes.

These geological records again support that the CH_4-G2a fraction results from the anti-phase changes of the northern and southern tropical monsoon wetlands, yielding a strong semi-precession frequency at ~10 ka. It is worthy

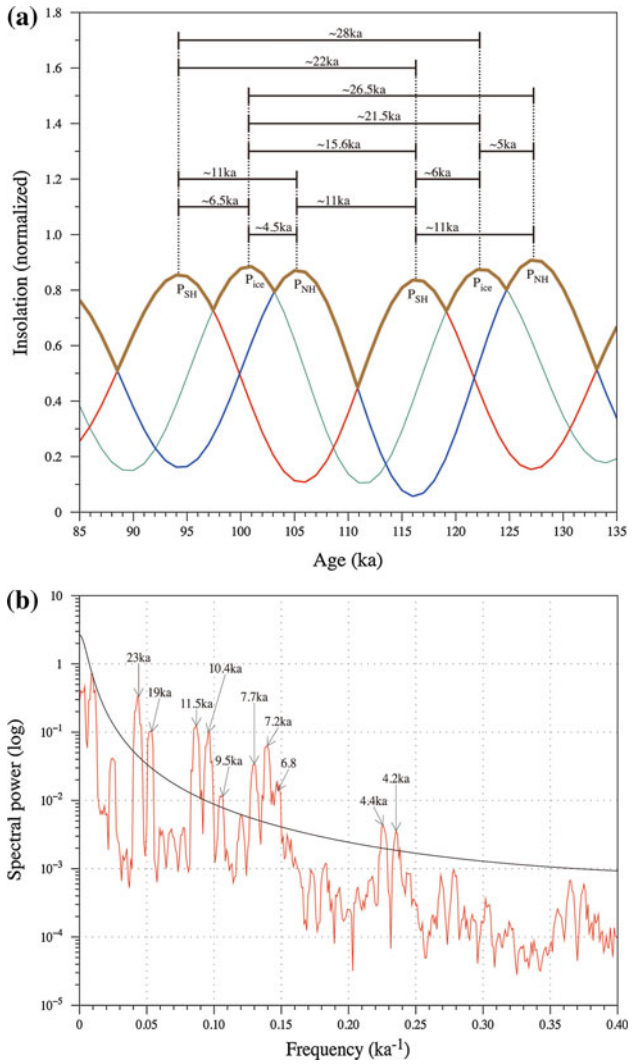

Fig. 9 Millennial CH_4 signals related with the combined effect of northern (P_{NH}) and southern (P_{SH}) insolation and glacial-interglacial (P_{ice}) changes at the precession bands. N30° summer insolation (normalized to 0–1), S30° summer insolation (normalized to 0–1), and the precession parameter (inversed, lagged and normalized to 0–1) are used to represent P_{NH}, P_{SH} and P_{ice} (3P), respectively. The time evolution of their maximum values is defined as the 3P curve. Because late Pleistocene LR04 $\delta^{18}O$ lags the precession by ~4.8 ka at the 23-ka band, and by ~2.8 ka at the 19-ka band in average (Lisiecki and Raymo 2005), a 4.8-ka lag to the precession is assumed here for P_{ice} to represent the ice volume component at the precession band. **a** Scheme showing the 3P-related CH_4 periods taking the 85–135 ka BP interval as an example. *Blue*, *red* and *green curves* indicate P_{NH}, P_{SH} and P_{ice}, respectively. *Thick brown line* represents the 3P curve. **b** MTM spectrum (*red*) of the 3P curve (0–800 ka BP interval) showing clear millennial periods centered at ~7.2 and 4.3 ka. *Black line* indicates the 99% confidence level

noting that CH_4-G2a peaks matching the northern insolation are generally stronger than those of the southern origin, confirming a more important role of the Northern Hemisphere, probably because of the stronger northern hemispheric monsoons. However, this is not regular with some southern peaks fairly intense. MIS-7 is a spectacular example, as shown by the CH_4-G2a peaks 18–21 in Fig. 5.

3.3 A plausible mechanism for the millennial methane signals

The millennial CH_4 components (CH_4-G2b), sometimes with large amplitudes, are rather comparable between EDC and Vostok (Figs. 4, 6a) in terms of CH_4 events. This indicates that CH_4-G2b contains true CH_4 signals dominating the noises. They mainly reside in PC24-80 (Fig. 3b) for EDC with ~8.2, 7.2, 6.6, 6, 5.5 and 4.2 ka periods after the bi-hemispheric insolation tuning (BHIT) (Fig. 6b). Their origins are much less known and considered part of the major challenges (Wolff and Spahni 2007; Wolff 2011).

Precession harmonics may lead to ~10 and ~5.5-ka frequencies for equatorial regions (Berger et al. 2006) with the signals rapidly weaken towards higher latitudes. Precession forcing may also generate a ~8.4-ka cycle for equatorial regions of which the signals could be transferred to subpolar regions (McIntyre and Molfino 1996). The ~8.2 and ~5.5-ka periods in the CH_4 record (Fig. 6b) are likely attributable to these precession-related processes in the equatorial regions. However, the millennial CH_4 changes, with the frequencies ranging between ~7.2 and ~6 ka and at ~4.2 ka (Fig. 6b), have to be explained by other mechanisms.

Section 3.1 shows that ice volume and CH_4-G1 are nearly in-phase at the eccentricity, obliquity and precession (23 and 19-kyr) frequencies (Fig. 3c). Geological evidence summarized in Sect. 3.2 shows that tropical CH_4 emissions in the two hemispheres are approximately in-phase with the precession-induced northern (P_{NH}) and southern (P_{SH}) insolation changes (Fig. 5). Because ice volume of the last 800 ka averagely lags the precession by ~4.8 ka at the 23-ka band, and ~2.8 ka at the 19-ka band (P_{ice}), respectively (Lisiecki and Raymo 2005), these three drivers (P_{NH}, P_{SH} and P_{ice}, referred to as 3P here), all varying at the precession bands, but with different phases to the precession (Fig. 9), would have left their imprints in the atmospheric CH_4 signals.

Assuming an ice volume lag of 4.8–2.8 ka to the precession, the 3P consecutive effects theoretically produce CH_4 periods at ~30–26, ~16–12, ~8–5.5, ~4.9–2.8 ka (Fig. 9a). Their exact values are slightly variable due to the two precession frequencies (23 and 19-kyr). They may also be affected by the possible phase instability between ice volume and insolation. For example, except the 23, 19 and ~10-ka periods, other main CH_4 frequencies between 90 and 130 ka BP may include the ~28, ~26.5, ~15.6, ~6.6, ~6, ~5 and ~4.5-ka signals (Fig. 9b) if a 4.8-ka

lag of ice volume to the precession is assumed. The effects of P_{ice} and P_{NH} may yield peaks at ~28, ~15.6, ~5 and ~4.5 ka and those of P_{ice} and P_{SH} may generate the others.

The main millennial signals, as well as some longer-term periods resolved in the bi-hemispheric insolation tuned CH_4 record (Fig. 6b) strikingly match these 3P-produced frequencies (Fig. 9b). Within the accuracy of the timescales, CH_4 period at ~4.2 ka is attributable to the combined effects of P_{ice} and P_{NH} while those between ~7.2 and ~6 ka and around ~13 ka are attributable to P_{ice} and P_{SH}. The ~28-ka period may relate to either the P_{ice}-P_{NH} effects or the P_{ice}-P_{SH} effects.

Thus, the millennial oscillatory signals of CH_4 are likely explainable by the combination of precession-related equatorial processes (McIntyre and Molfino 1996; Berger et al. 2006) and by the effects of insolation and ice-volume at the precession bands. Other climate proxies related to bi-hemispheric insolation and ice volume changes would also bear these signals although the mechanisms may be different. For example, 8–3-ka periods are likely characteristic for geological records related with ENSO (Wang et al. 2005).

Although P_{ice} is related with northern insolation, its effect should be roughly synchronous at the global scale along the glacial-interglacial cycles according to the Milankovitch rule (Milankovitch 1948). Figures 4 and 5 show that millennial CH_4 signals are visually stronger during the last 400 ka than for the 400–800 ka interval, such that CH_4-G2a between 400 and 800 ka BP appears to be more purely linked with bi-hemispheric insolation (Fig. 5). These suggest a reinforced P_{ice} effect since ~400 kyr BP, as is consistent with the global ice volume increase after the mid-Brunhes Event (Lisiecki and Raymo 2005; Jouzel et al. 2007). These features are again supportive to our tentative interpretation about the millennial CH_4 signals.

3.4 Methane cycle and global monsoon

The above analyses show that atmospheric CH_4 variability in the past 800 ka are fundamentally attributable to three main drivers: (1) the glacial-interglacial changes through modulating the water cycle and temperatures at all latitudes in both hemispheres (~80% variance); (2) tropical monsoons in response to the low latitude summer insolation changes in both hemispheres (~15% variance); and (3) the precession-related equatorial processes and the combined effects of bi-hemispheric insolation and ice volume at the precession bands (~5% variance). All these CH4 fractions are bi-hemispheric in nature. Although the phase of CH_4-G1 is closer to northern insolation changes (Fig. 3c) due to the northern insolation controls on the glacial-interglacial cycles, it also derives from both southern and northern hemispheric wetlands, rather than from the Northern Hemisphere alone.

As a further evaluation of these interpretations, we use a stack of marine $\delta^{18}O$, northern and southern low latitude insolation timeseries to model the main features of CH_4 changes (Fig. 10a). Because the strong variance instability over time, it is not yet possible to consider the weight of each driver in this simple stack. However, the stacked curve produces a timeseries with the orbital and millennial-scale peaks matching those in the EDC CH_4 record (Fig. 10a), as are confirmed by the high coherencies between the two timeseries at these frequencies (Fig. 10b). These strongly support our causal attributions of the different CH_4 signals even though the amplitudes are not considered. Numerical modeling accounting these insights and the nonlinearity of CH_4 responses to the above drivers (i.e. the variance changes through time) would yield much better results, in particular, with regards to the amplitude variability.

Although the glacial-interglacial components explain ~80% of the CH_4 variability in average, our results suggest that boreal wetlands is not the primary modulator to the CH_4 record. At the present interglacial time when boreal CH_4 sources are most active, their contribution to global CH_4 emission represents only ~40% (Cao et al. 1996; Lehner and Doll 2004) (Fig. 1c). The other ~60% is mainly from monsoonal wetlands since other non-monsoonal wetlands are minor in proportion (Fig. 1). This further implies that boreal emission should mostly not exceed ~40% during the glacial-interglacial cycles because boreal sources were further reduced in interstadial periods and essentially shut down in glacial periods (Landais et al. 2010).

Among the ~80% glacial-interglacial variance in the CH_4 records (CH_4-G1), boreal sources should share about the half if their modern contribution is averagely assumed for the past. Accordingly, the other half part of glacial-interglacial CH_4 signals has to be attributed to wetlands beyond boreal regions. Although they include tropical monsoon regions, monsoonal and non-monsoonal zones at mid latitudes, monsoon-related wetlands certainly contribute the most to the latter half of CH_4-G1, given that wetlands beyond monsoon and boreal regions are minor in proportion (Fig. 1). The case of MIS-13 discussed in Sect. 3.1 is indeed another support to the role of monsoon wetlands on CH_4-G1 because high latitude wetlands are scarce in the Southern Hemisphere (Fig. 1).

Low latitude summer insolation in both hemispheres account totally for ~20% of CH_4 variability, firstly through modulating the tropical monsoons (CH_4-G2a, ~15%) and secondly through the equatorial processes (McIntyre and Molfino 1996; Berger et al. 2006) and the combined effects of 3P (CH_4-G2b, ~5%). Today, tropical

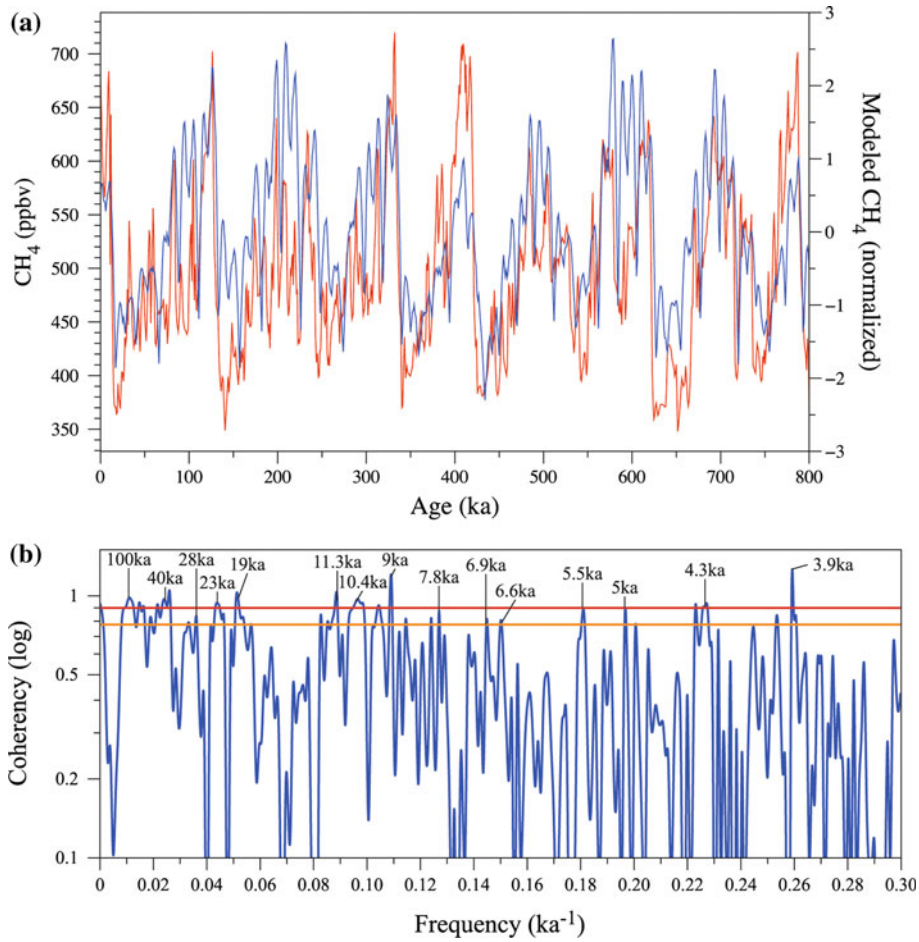

Fig. 10 Comparison of CH_4 record with the modeled CH_4 timeseries. **a** Modeled CH_4 (*blue*) derived from a stack of LR04 $\delta^{18}O$ (Lisiecki and Raymo 2005), BHI (see Fig. 5) and 3P (see Fig. 9) representing the three main CH_4 drivers discussed in this study. The timeseries are normalized, summed and then normalized again. EDC CH_4 (*red*, vs. BHIT) is shown for comparison. The model has not been able to consider the relative variance of CH_4 drivers because of their strong variability over time, but has captured most of the EDC CH_4 peaks at both orbital and millennial scales. **b** Coherency between modeled CH_4 and EDC CH_4 (vs. BHIT). *Red* and *orange horizontal lines* indicate the 99 and 95% confidence levels, respectively. High coherency values are obtained at the discussed orbital and millennial bands

wetlands account for ~60% of the global CH_4 emission (Fig. 1), but our analyses show a total variance of only ~20% (CH_4-G2) linkable with low latitude insolation. These rightly suggest that a greater part of the CH_4 variance is attributable to the glacial-interglacial modulations on the tropical wetlands via the processes discussed in Sect. 3.1.

The glacial-interglacial controls on the tropical monsoon rainfall and wetlands are strongly supported by the eolian dust data (Fig. 7) from tropical Africa (deMenocal 1995), tropical Arabia and Somalia (Clemens et al. 1991, 1996) and northern South America (Winckler et al. 2008), and by the vegetation changes at wetsern Amazonia following the glacial-interglacial cycles (Cardenas et al. 2011). These regions are all under strong influences of tropical monsoons, but continental humidity changes within the monsoon zones, primarily linked with monsoon rainfall, also display clear glacial-interglacial signals (Fig. 7) even though the strengths of tropical monsoon winds may dominantly vary at the precession rhythms of summer insolation. Glacial-interglacial controls on moisture availability may be mainly responsible for these features of the tropical monsoons. This interpretation is congruent with the grain-size monsoon record (wind strength) and the dust flux record (continental humidity) indicative of the tropical monsoon zones (Clemens et al. 1991, 1996; deMenocal 1995). These imply that tropical monsoons, particularly in term of rainfall, also bear a glacial-interglacial component despite of the relatively weak magnitudes.

The above estimates of variances only represent the approximate means because the relative variance of each driver is variable over time, as is shown by the amplitude changes of the CH_4-G1, G2a and G2b timeseries (Figs. 4, 5). For example, glacial CH_4 emissions from boreal wetlands should be most shut down during which tropical wetlands should play a primary role. The role of the Southern Hemisphere climate during MIS-13 is more accentuated than for the other interglacials due to the strong asymmetry of hemispheric climates (Guo et al. 2009).

Since nearly half of CH_4-G1, the most of CH_4-G2 are monsoon-related, the results in this study also suggest that the integration of regional monsoons, if viewed as a global system (global monsoon)(Wang 2009), would consist of two main integrated components, one roughly anti-phasing between the two hemispheres primarily driven by the ITCZ

oscillations in response to the low-latitude summer insolation changes (the ITCZ monsoon component), and another rough-synchronously modulated by the glacial-interglacial cycles at the global scale (the glacial-interglacial monsoon component). Global monsoon rainfall should be ultimately determined by the integration of these two components, and controls the monsoon wetlands and their CH_4 emissions.

Both chemical weathering of the loess-soil sequences in northern China (Guo et al. 2000) and the stalagmite $\delta^{18}O$ records from southern China (Wang et al. 2008) are interpreted as proxies of East Asian monsoon. However, their orbital signatures are quite different. Loess weathering records contain prominent glacial-interglacial signals (Fig. 2a) while stalagmite $\delta^{18}O$ is dominated by the ~20-ka precession period (Fig. 8a). Our interpretations provide a likely explanation on this difference: the stalagmite $\delta^{18}O$ records, mostly recovered from low latitude Asia (Fig. 8), are more indicative of the ITCZ monsoon component while the loess-soil records are more indicative of the glacial-interglacial monsoon component.

As discussed in detail in Sect. 3.1, besides the moisture availability that affect monsoonal rainfall at both low and mid-latitudes, other main processes introducing the glacial-interglacial signals into the loess records include the changes in tropical SST, seal-level (shoreline distance), the thermal conditions of Tibetan Plateau and in the seasonality related with the Asian winter monsoon. These factors are strongly modulated by the glacial-interglacial boundary conditions. The weak glacial-interglacial signals in stalagmite $\delta^{18}O$ might also be partially attributable to the moisture sources from the Indian Ocean (Pausata et al. 2011), such that it may better reflect tropical monsoon events than for monsoon rainfall changes.

Atmospheric CH_4 record is sometimes used to infer the strengths of regional monsoon circulations (Ziegler et al. 2010). This utility is clearly compromised by the bi-hemispheric nature of CH_4 and by the significant non-monsoonal contributions mainly from boreal wetlands. CH_4 record can be used as a proxy of monsoon only if all regional monsoon circulations are viewed as a global system, i.e. global monsoon (Wang 2009), given that no better proxy is available and that the contribution of monsoonal wetlands is unlikely to be less than 60% of the global CH_4 emission in the past 800 ka.

4 Tropical monsoons and the Holocene methane trends

During the Holocene, CH_4 gradually decreased from ~680 to ~570 ppbv between 10 and 5 ka BP (Fig. 8b) and then reversed the trend since ~5 ka ago with a preindustrial level of ~680 ppbv (Chappellaz et al. 1993; Petit et al. 1999; Spahni et al. 2005; Loulergue et al. 2008). The early anthropogenic hypothesis (Ruddiman and Thomson 2001; Ruddiman 2003, 2007) attributes the CH_4 decrease in the early part of the Holocene to weakened northern hemispheric monsoons, and suggest that early rice-irrigation and methane-emitting livestock have significantly contributed to the mid-Holocene CH_4 reversal and subsequent rise.

Although controversies still persist relative to this *V-shape* CH_4 trend for the Holocene (Fig. 8b), several lines of evidence tend to support an early anthropogenic impact. A compilation of archeological sites in rice-growing regions of China show that the number of new rice-planting sites between 6,000 and 4,000 years ago increased almost tenfold compared with those during previous millennia (Ruddiman et al. 2008). A recent compilation of rice-irrigation and livestock data throughout the Old Word (Fuller et al. 2011) is also congruent with an anthropogenic source of later Holocene CH_4. These indicate that human interventions have figured in the Holocene CH_4 reversal and the subsequent CH_4 rise.

Besides the anthropogenic sources, the analyses in this study show that the weakened northern monsoons and the strengthened southern tropical monsoons have also contributed to the *V-shape* CH_4 trend of the Holocene. Figures 4 and 5 show that similar *V-shape* trends near-systematically occurred in the CH_4-G2 fraction over the past 800 ka, roughly once every 10,000 years, as are more clearly seen in the CH_4 records in comparing CH_4-G2 with the original CH_4 timeseries (Fig. 5).

These *V-shape* trends closely match the bi-hemispheric insolation (Fig. 5), and the anti-phase changes of monsoon events recorded by stalagmite $\delta^{18}O$ from Asia (Wang et al. 2008) and South America (Wang et al. 2004) (Fig. 8). The Holocene CH_4 changes (Fig. 8b) correspond to the last *V-shape* of CH_4-G2a (Figs. 4, 5). This observation is consistent with the reduced inter-hemispheric CH_4 gradient in the late Holocene (Chappellaz et al. 1997a; Brook et al. 2000) that supports a tropical and subtropical origin of the CH_4 increase, instead of a high latitude origin.

CH_4 varied between ~350 and ~710 ppbv following the glacial-interglacial cycles. The *V-shape* changes of CH_4-G2a represent an average variance of ~15% although it varies over time. Assuming this average variance for the Holocene, its contribution to the CH_4 reversal would be ~54 ppbv. Given that CH_4-G2b (~5% variance) also mostly originates from tropical monsoons as discussed in Sect. 3.2, a total variance of ~20% would account for ~72 ppbv, a value still smaller than the late Holocene CH_4 rise. Consequently, human interventions cannot be ruled out for explaining the total CH_4 rise in the late Holocene unless a greater variance is assigned for CH_4-G2a for the Holocene.

The causes for the CH_4-G2a variance changes over time need further studies. The *V-shape* trends of CH_4-G2a at the semi-precession frequency are more accentuated during some interglacials, for example, during MIS-7, the Holocene and some glacial times (Figs. 4, 5). In contrast, they are relatively weaker in some other interglacials. These may be attributed to the differences in various boundary conditions among which ice-volume changes (Singarayer et al. 2011) are worthy particular attentions. Because $\sim$80% of the atmospheric CH_4 signals is attributable to glacial-interglacial cycles, tropical monsoon-related CH_4 signals are naturally accentuated when the changes in ice-volume are small. During the Holocene, the relatively small decrease of ice-volume (Lisiecki and Raymo 2005), associated with the human intervention (Ruddiman et al. 2008) would have accentuated the *V-shape* CH_4 trends.

5 Conclusions

Understanding the causes of atmospheric CH_4 changes are helpful for exploring the relationships between greenhouse gases and climate, for accurately dating marine and ice records (Ruddiman and Raymo 2003), for assessing the monsoon dynamics particularly if monsoon is viewed as a global system (global monsoon) (Wang 2009), and for evaluating human impacts on the climate system (Ruddiman 2007).

Timeseries analyses on the Antarctic CH_4 records and correlations with geological records in this study show that atmospheric CH_4 changes bear three main groups of signals attributable to different drivers: (1) a glacial-interglacial forced component (CH_4-G1) with a total variance of $\sim$80%, (2) a bi-hemispheric insolation driven component (CH_4-G2a, $\sim$15% variance) through modulating the southern and northern tropical monsoons, and (3) a millennial oscillatory component (CH_4-G2b, $\sim$5% variance) seemingly attributable to precession-related equatorial processes and to the combined effect of ice volume and insolation at the precession bands. Although the contribution estimates of the drivers may not be sufficiently accurate and the variance of each fraction varies over time, they provide helpful insights about the main origins of CH_4 signals.

Clearly, the glacial-interglacial cycle is a primary driver of atmospheric CH_4 changes. Our results indicate that both monsoonal and non-monsoonal wetlands at all latitudes in both hemispheres share these effects. Main mechanisms include the glacial-interglacial influences on boreal wetlands, global moisture availability, temperature changes, and the monsoon rainfall. Besides boreal wetlands, monsoon regions have played a prominent role in introducing the glacial-interglacial signals into the past CH_4 records.

The anti-phase tropical monsoon changes at the precession band, mainly in response to the low latitude summer insolation of the two hemispheres, are another prominent driver of CH_4 in the past 800 ka. This supports a more important role of the Southern Hemisphere to CH_4 than previously believed, and is consistent with the recent CH_4 modeling for the Holocene (Singarayer et al. 2011). This mechanism led to the precession and semi-precession periods among the main CH_4 cycles, and also partially explains the Holocene CH_4 reversal and subsequent rise since $\sim$5,000 years ago besides the human intervention. This bi-hemispheric rational would have also the potential for refining ice-core age models.

The origins of millennial-scale CH_4 changes are much less known (Wolff 2011). Part of the signals are likely attributable to precession-related climate processes in equatorial regions (McIntyre and Molfino 1996; Berger et al. 2006). Our results suggest that past atmospheric CH_4 changes contain three parts of precession signals, respectively related with ice volume changes at the precession band, low latitude summer insolation of both Southern and Northern Hemispheres. The millennial oscillatory components of CH_4 are seemingly related with the consecutive effects of these three precession-rhythm drivers. This mechanism would also account for some longer-term CH_4 periods at $\sim$30–28 and $\sim$16–14 ka.

Because nearly half of CH_4-G1, the most of CH_4-G2a and a large part of CH_4-G2b are monsoon-related, our results also suggest that global monsoon (Wang 2009) can be regarded as a system consisting of two main integrated components, one primarily driven by the ITCZ oscillations in response to the low-latitude summer insolation changes, roughly anti-phase between the two hemispheres (the ITCZ monsoon component); and another modulated by the glacial-interglacial cycles, mostly synchronous at the global scale (the glacial-interglacial monsoon component). At best, atmospheric CH_4 records can be described as the only proxy that integrates all wetland processes, including the important effects of changes in monsoonal circulations of both hemispheres and the non-monsoonal contributions mainly from boreal wetlands. Up to date, it is the only and probably the best proxy available for documenting the past changes of global monsoon. However, the utility of CH_4 as a proxy of monsoon changes at any specific location is compromised by its bi-hemispheric nature.

Acknowledgments This study is supported by the National Basic Research Program of China (2010CB950200) and the National Natural Science Foundation of China (40730104). Thanks are extended to Prof. W. F. Ruddiman and Prof. P. X. Wang for constructive advices and discussions. We also thank the two anonymous reviewers for their comments and suggestions that have greatly improved the manuscript.

References

Adegbie AT, Schneider RR, Rohl U, Wefer G (2003) Glacial millennial-scale fluctuations in central African precipitation recorded in terrigenous sediment supply and freshwater signals offshore Cameroon. Palaeogeogr Palaeoecol Palaeocl 197:323–333

Aselmann I, Crutzen PJ (1989) Global distribution of natural freshwater wetlands and rice paddies, their net primary productivity, seasonality and possible methane emissions. J Atmos Chem 8:307–358

Barker P, Williamson D, Gasse F, Gibert E (2003) Climatic and volcanic forcing revealed in a 50,000-year diatom record from Lake Massoko, Tanzania. Quat Res 60:368–376

Bartlett KB, Harriss RC (1993) Review and assessment of methane emissions from wetlands. Chemosphere 26:261–320

Bassinot FC, Labeyrie LD, Vincent E, Quidelleur X, Shackleton NJ, Lancelot Y (1994) The astronomical theory of climate and the age of the Brunhes-Matuyama magnetic reversal. Earth Planet Sci Lett 126:91–108

Becquey S, Gersonde R (2003) A 0.55-Ma paleotemperature record from the Subantarctic zone: implications for Antarctic Circumpolar Current development. Paleoceanography 18:1014. doi:10.1029/2000PA000576

Beerling D, Berner RA, Mackenzie FT, Harfoot MB, Pyle JA (2009) Methane and the CH_4 related greenhouse effect over the past 400 million years. Am J Sci 309(2):97–113. doi:10.2475/02.2009.01

Berger A (1978) Long-term variations of daily insolation and Quaternary climate changes. J Atmos Sci 35:2362–2367

Berger A, Loutre MF, Melice JL (2006) Equatorial insolation: from the precession harmonics to eccentricity frequencies. Clim Past 2:131–136

Bonnefille R, Chalié F (2000) Pollen-inferred precipitation time-series from equatorial mountains, Africa, the last 40 kyr BP. Global Planet Change 26:25–50

Brook EJ (2009) Palaeoclimate atmospheric carbon footprints? Nat Geosci 2:170–172

Brook EJ, Harder S, Severinghaus J, Steig EJ, Sucher CM (2000) On the origin and timing of rapid changes in atmospheric methane during the last glacial period. Global Biogeochem Cycle 14:559–572

Cao MK, Marshall S, Gregson K (1996) Global carbon exchange and methane emissions from natural wetlands: application of a process-based model. J Geophys Res Atmos 101:14399–14414

Cardenas ML, Gosling WD, Sherlock SC, Poole I, Pennington RT, Mothes P (2011) The response of vegetation on the Andean Flank in Western Amazonia to Pleistocene climate change. Science 331(6020):1055–1058. doi:10.1126/science.1197947

Chappellaz J, Blunier T, Raynaud D, Barnola JM, Schwander J, Stauffer B (1993) Synchronous changes in atmospheric CH_4 and Greenland climate between 40 and 8 kyr BP. Nature 366:443–445

Chappellaz J, Blunier T, Kints S, Dallenbach A, Barnola JM, Schwander J, Raynaud D, Stauffer B (1997a) Changes in the atmospheric CH_4 gradient between Greenland and Antarctica during the Holocene. J Geophys Res Atmos 102:15987–15997

Chappellaz J, Brook E, Blunier T, Malaize B (1997b) CH_4 and $\delta^{18}O$ of O_2 records from Antarctic and Greenland ice: a clue for stratigraphic disturbance in the bottom part of the Greenland Ice Core Project and the Greenland Ice Sheet Project 2 ice cores. J Geophys Res Oceans 102:26547–26557

Chen FH, Bloemendal J, Zhang PZ, Liu GX (1999) An 800 ky proxy record of climate from lake sediments of the Zoige Basin, eastern Tibetan Plateau. Palaeogeogra Palaeoecol Palaeocl 151:307–320

Clemens S, Prell W, Murray D, Shimmield G, Weedon G (1991) Forcing mechanisms of the Indian-Ocean monsoon. Nature 353:720–725

Clemens SC, Murray DW, Prell WL (1996) Nonstationary phase of the Plio-Pleistocene Asian monsoon. Science 274:943–948. doi:10.1126/science.274.5289.943

Cosford J, Qing HR, Eglington B, Mattey D, Yuan DX, Zhang ML, Cheng H (2008) East Asian monsoon variability since the Mid-Holocene recorded in a high-resolution, absolute-dated aragonite speleothem from eastern China. Earth Planet Sci Lett 275:296–307

Cox PM, Harrie PP, Huntingford C, Betts RA, Collins M, Jones CD, Jupp TE, Marengo JA, Nobre CA (2008) Increasing risk of Amazonian drought due to decreasing aerosol pollution. Nature 453:212–215

Crutzen PJ, Aselmann I, Seil W (1986) Methane production by domestic animals, wild ruminants, other herbivorous fauna, and human. Tellus B 38:271–284

Cruz FW, Burns SJ, Karmann I, Sharp WD, Vuille M, Cardoso AO, Ferrari JA, Dias PLS, Viana O (2005) Insolation-driven changes in atmospheric circulation over the past 116,000 years in subtropical Brazil. Nature 434:63–66

de Garidel-Thoron T, Rosenthal Y, Bassinot F, Beaufort L (2005) Stable sea surface temperatures in the western Pacific warm pool over the past 1.75 million years. Nature 433:294–298

de Vernal A, Hillaire-Marcel C (2008) Natural variability of Greenland climate, vegetation, and ice volume during the past million years. Science 320:1622–1625

deMenocal PB (1995) Plio-Pleistocene African climate. Science 270:53–59

Ding ZT, Liu TS, Rutter NW, Yu ZW, Guo ZT, Zhu RX (1995) Ice-volume forcing of East Asian winter monsoon variations in the past 800,000 years. Quat Res 44(2):149–159

Ding YH, Li CY, Liu YJ (2004) Overview of the South China Sea monsoon experiment. Adv Atmos Sci 21(3):343–360. doi:10.1007/bf02915563

Fawcett PJ, Werne JP, Anderson RS, Heikoop JM, Brown ET, Berke MA, Smith SJ, Goff F, Donohoo-Hurley L, Cisneros-Dozal LM, Schouten S, Sinninghe Damste JS, Huang Y, Toney J, Fessenden J, WoldeGabriel G, Atudorei V, Geissman JW, Allen CD (2011) Extended megadroughts in the southwestern United States during Pleistocene interglacials. Nature 470(7335):518–521

Fischer H, Behrens M, Bock M, Richter U, Schmitt J, Loulergue L, Chappellaz J, Spahni R, Blunier T, Leuenberger M, Stocker TF (2008) Changing boreal methane sources and constant biomass burning during the last termination. Nature 452:864–867

Fuller DQ, van Etten J, Manning K, Castillo C, Kingwell-Banham E, Weisskopf A, Qin L, Sato Y-I, Hijmans RJ (2011) The contribution of rice agriculture and livestock pastoralism to prehistoric methane levels: an archaeological assessment. Holocene. doi:10.1177/0959683611398052

Gamiz-Fortis SR, Pozo-Vazquez D, Esteban-Parra MJ, Castro-Diez Y (2002) Spectral characteristics and predictability of the NAO assessed through Singular Spectral Analysis. J Geophys Res Atmos 107:4685. doi:10.1029/2001JD001436

Gasse F (2000) Hydrological changes in the African tropics since the Last Glacial Maximum. Quat Sci Rev 19:189–211

Ghil M, Allen MR, Dettinger MD, Ide K, Kondrashov D, Mann ME, Robertson AW, Saunders A, Tian Y, Varadi F, Yiou P (2002) Advanced spectral methods for climatic timeseries. Rev Geophys 40:1003. doi:10.1029/2000RG000092

Griffiths ML, Drysdale RN, Gagan MK, Zhao JX, Ayliffe LK, Hellstrom JC, Hantoro WS, Frisia S, Feng YX, Cartwright I, Pierre ES, Fischer MJ, Suwargadi BW (2009) Increasing Australian-Indonesian monsoon rainfall linked to early Holocene sea-level rise. Nat Geosci 2:636–639

Guo ZT, Liu TS, Fédoroff N, Wei LY, Ding ZL, Wu NQ, Lu HY, Jiang WY, An ZS (1998) Climate extremes in loess of China coupled with the strength of deep-water formation in the North Atlantic. Glob Planet Change 18(3–4):113–128

Guo ZT, Biscaye P, Wei LY, Chen XH, Peng SZ, Liu TS (2000) Summer monsoon varatiations over the last 1.2 Ma from the weathering of loess-soil sequences in China. Geophys Res Lett 27:1751–1754

Guo ZT, Peng SZ, Hao QZ, Biscaye PE, An ZS, Liu TS (2004) Late Miocene-Pliocene development of Asian aridification as recorded in the Red-Earth Formation in northern China. Glob Planet Change 41(3–4):135–145. doi:10.1016/j.gloplacha.2004.01.002

Guo ZT, Berger A, Yin QZ, Qin L (2009) Strong asymmetry of hemispheric climates during MIS-13 inferred from correlating China loess and Antarctica ice records. Clim Past 5:21–31

Halley E (1986) An historical account of the trade winds and monsoons observable in the seas between and near the tropics with an attempt to assign the physical cause of the said wind. Phil Trans R Soc Lond 16:153–168

Haug GH, Hughen KA, Sigman DM, Peterson LC, Rohl U (2001) Southward migration of the intertropical convergence zone through the Holocene. Science 293:1304–1308

Horikawa K, Murayama M, Minagawa M, Kato Y, Sagawa T (2010) Latitudinal and downcore (0–750 ka) changes in n-alkane chain lengths in the eastern equatorial Pacific. Quat Res 73(3):573–582. doi:10.1016/j.yqres.2010.01.001

Hovan SA, Rea DK, Pisias NG, Shackleton NJ (1989) A direct link between the China loess and marine $\delta^{18}O$ records—Aeolian flux to the North Pacific. Nature 340:296–298

Huffman GJ, Adler RF, Bolvin DT, Gu G (2009) Improving the global precipitation record: GPCP Version 2.1. Geophys Res Lett 36(17):L17808. doi:10.1029/2009gl040000

Hutchinson GE (1954) The biochemistry of the terrestrial atmosphere. In: Kuiper GP (ed) The solar system. Chcago Press, Chicago, pp 371–433

Iriondo M (2000) Patagonian dust in Antarctica. Quat Int 68:83–86

Jiang DB, Lang XM (2010) Last Glacial Maximum East Asian monsoon: results of PMIP simulations. J Clim 23:5030–5038

Jouzel J, Masson-Delmotte V, Cattani O, Dreyfus G, Falourd S, Hoffmann G, Minster B, Nouet J, Barnola JM, Chappellaz J, Fischer H, Gallet JC, Johnsen S, Leuenberger M, Loulergue L, Luethi D, Oerter H, Parrenin F, Raisbeck G, Raynaud D, Schilt A, Schwander J, Selmo E, Souchez R, Spahni R, Stauffer B, Steffensen JP, Stenni B, Stocker TF, Tison JL, Werner M, Wolff EW (2007) Orbital and millennial Antarctic climate variability over the past 800,000 years. Science 317:793–796

Kaplan JO (2002) Wetlands at the Last Glacial Maximum: distribution and methane emissions. Geophys Res Lett 29(6):1079. doi:10.1029/2001gl013366

Kaplan JO, Folberth G, Hauglustaine DA (2006) Role of methane and biogenic volatile organic compound sources in late glacial and Holocene fluctuations of atmospheric methane concentrations. Glob Biogeochem Cycles 20:GB2016. doi:10.1029/2005GB002590

Karl DM, Beversdorf L, Bjorkman KM, Church MJ, Martinez A, DeLong EF (2008) Aerobic production of methane in the sea. Nat Geosci 1:473–478

Kelly MJ, Edwards RL, Cheng H, Yuan D, Cai Y, Zhang M, Lin Y, An Z (2006) High resolution characterization of the Asian Monsoon between 146,000 and 99,000 years B.P. from Dongge Cave, China and global correlation of events surrounding Termination II. Palaeogeogra Palaeoecol Palaeocl 236:20–38

Keppler F, Hamilton JTG, Brass M, Rockmann T (2006) Methane emissions from terrestrial plants under aerobic conditions. Nature 439:187–191

King AL, Howard WR (2000) Middle Pleistocene sea-surface temperature change in the southwest Pacific Ocean on orbital and suborbital time scales. Geology 28:659–662

Kukla G (1987) Loess stratigraphy in central China. Quat Sci Rev 6:191–219

Kutzbach JE (1981) Monsoon climate of the early Holocene—climate experiment with the earths orbital parameters for 9,000 years ago. Science 214:59–61

Kutzbach JE, Liu Z (1997) Response of the African monsoon to orbital forcing and ocean feedbacks in the middle Holocene. Science 278:440–443

Lambert F, Delmonte B, Petit JR, Bigler M, Kaufmann PR, Hutterli MA, Stocker TF, Ruth U, Steffensen JP, Maggi V (2008) Dust-climate couplings over the past 800,000 years from the EPICA Dome C ice core. Nature 452:616–619

Landais A, Dreyfus G, Capron E, Masson-Delmotte V, Sanchez-Goni MF, Desprat S, Hoffmann G, Jouzel J, Leuenberger M, Johnsen S (2010) What drives the millennial and orbital variations of $\delta^{18}O_{atm}$? Quat Sci Rev 29:235–246

Lehner B, Doll P (2004) Development and validation of a global database of lakes, reservoirs and wetlands. J Hydrol 296:1–22

Lestari RK, Iwasaki T (2006) A GCM study on the roles of the seasonal marches of the SST and land-sea thermal contrast in the onset of the Asian summer monsoon. J Meteorol Soc Jpn 84:69–83

Li Q, Wang P, Zhao Q, Tian J, Cheng X, Jian Z, Zhong G, Chen M (2008) Paleoceanography of the mid-Pleistocene South China Sea. Quat Sci Rev 27:1217–1233

Lisiecki LE, Raymo ME (2005) A Pliocene–Pleistocene stack of 57 globally distributed benthic $\delta^{18}O$ records. Paleoceanography 20:PA1003. doi:10.1029/2004PA001071

Liu TS, Guo ZT, Liu JQ, Han JM, Ding ZL, Gu ZY, Wu NQ (1995) Variations of eastern Asian monsoon over the last 140,000 years. Bull Soc Geol France 166:221–229

Loulergue L, Schilt A, Spahni R, Masson-Delmotte V, Blunier T, Lemieux B, Barnola JM, Raynaud D, Stocker TF, Chappellaz J (2008) Orbital and millennial-scale features of atmospheric CH4 over the past 800,000 years. Nature 453:383–386

Luthi D, Le Floch M, Bereiter B, Blunier T, Barnola JM, Siegenthaler U, Raynaud D, Jouzel J, Fischer H, Kawamura K, Stocker TF (2008) High-resolution carbon dioxide concentration record 650,000–800,000 years before present. Nature 453:379–382

Magee JW, Miller GH, Spooner NA, Questiaux D (2004) Continuous 150 ky monsoon record from Lake Eyre, Australia: insolation-forcing implications and unexpected Holocene failure. Geology 32:885–888

Markgraf V, Baumgartner TR, Bradbury JP, Diaz HF, Dunbar RB, Luckman BH, Seltzer GO, Swetnam TW, Villalba R (2000) Paleoclimate reconstruction along the Pole-Equator-Pole transect of the Americas (PEP 1). Quat Sci Rev 19:125–140

Marković SB, Hambach U, Catto N, Jovanović M, Buggle B, Machalett B, Zöller L, Glaser B, Frechen M (2009) The Middle and Late Pleistocene loess sequences at Batajnica, Vojvodina, Serbia. Quat Int 198:255–266

Martínez-Garcia A, Rosell-Melé A, Geibert W, Gersonde R, Masqué P, Gaspari V, Barbante C (2009) Links between iron supply, marine productivity, sea surface temperature, and CO_2 over the last 1.1 Ma. Paleoceanography 24(1):PA1207. doi:10.1029/2008pa001657

Matthews E, Fung I (1987) Methane emission from natural wetlands: global distribution, area, and environmental characteristics of sources. Glob Biogeochem Cycles 1:61–86

McClymont EL, Rosell-Mele A, Giraudeau J, Pierre C, Lloyd JM (2005) Alkenone and coccolith records of the mid-pleistocene in the south-east Atlantic: implications for the u-37(k) index and South African climate. Quat Sci Rev 24:1559–1572

McIntyre A, Molfino B (1996) Forcing of Atlantic equatorial and subpolar millennial cycles by precession. Science 274:1867–1870

McManus JF, Oppo DW, Cullen JL (1999) A 0.5-million-year record of millennial-scale climate variability in the North Atlantic. Science 283(5404):971–975

Milankovitch M (1948) Ausbau Und Gegenwartiger Stand Der Astronomischen Theorie Der Erdgeschichtlichen Klimate. Experientia 4(11):413–418

Min S-K, Zhang X, Zwiers FW, Hegerl GC (2011) Human contribution to more-intense precipitation extremes. Nature 470(7334):378–381

Mohtadi M, Lückge A, Steinke S, Groeneveld J, Hebbeln D, Westphal N (2010) Late Pleistocene surface and thermocline conditions of the eastern tropical Indian Ocean. Quat Sci Rev 29(7–8):887–896. doi:10.1016/j.quascirev.2009.12.006

Parrenin F, Barnola JM, Beer J, Blunier T, Castellano E, Chappellaz J, Dreyfus G, Fischer H, Fujita S, Jouzel J, Kawamura K, Lemieux-Dudon B, Loulergue L, Masson-Delmotte V, Narcisi B, Petit JR, Raisbeck G, Raynaud D, Ruth U, Schwander J, Severi M, Spahni R, Steffensen JP, Svensson A, Udisti R, Waelbroeck C, Wolff E (2007) The EDC3 chronology for the EPICA Dome C ice core. Clim Past 3:485–497

Partridge TC, deMenocal PB, Lorentz SA, Paiker MJ, Vogel JC (1997) Orbital forcing of climate over South Africa: A 200,000-year rainfall record from the Pretoria Saltpan. Quaternary Sci Rev 16:1125–1133

Pausata FSR, Battisti DS, Nisancioglu KH, Bitz CM (2011) Chinese stalagmite $\delta^{18}O$ controlled by changes in the Indian monsoon during a simulated Heinrich event. Nat Geosci 4:474–480. doi:10.1038/ngeo1169

Penland C, Ghil M, Weikmann K (1991) Adaptive filtering and maximum entropy spectra with application to changes in atmospheric angular momentum. J Geophys Res 96:22659–22671

Petit JR, Jouzel J, Raynaud D, Barkov NI, Barnola J-M, Basile I, Bender M, Chappellaz J, Davisk M, Delaygue G, Delmotte M, Kotlyakov VM, Legrand M, Lipenkov VY, Lorius C, Pepin L, Ritz C, Saltzman E, Stievenard M (1999) Climate and atmospheric history of the past 420,000 years from the Vostok ice core, Antarctica. Nature 399:429–436

Pisias NG, Clark PU, Brook EJ (2010) Modes of global climate variability during Marine Isotope Stage 3 (60–26 ka). J Clim 23:1581–1588

Poore RZ, Pavich MJ, Grissino-Mayer HD (2005) Record of the North American southwest monsoon from Gulf of Mexico sediment cores. Geology 33:209–212

Prokopenko AA, Williams DF, Kuzmin MI, Karabanov EB, Khursevich GK, Peck JA (2002) Muted climate variations in continental Siberia during the mid-Pleistocene epoch. Nature 418:65–68

Quay PD, King SL, Stutsman J, Wilbur DO, Steele LP (1991) Carbon isotope composition of CH_4: fossil and biomass burning source strengths. Glob Biogeochem Cycles 5:25–47

Rossignol-Strick M, Paterne M, Bassinot FC, Emeis KC, De Lange GJ (1998) An unusual mid-Pleistocene monsoon period over Africa and Asia. Nature 392:269–272

Ruddiman WF (2003) The anthropogenic greenhouse era began thousands of years ago. Clim Change 61:261–293

Ruddiman WF (2007) The early anthropogenic hypothesis: challenges and responses. Rev Geophys 45:RG4001. doi:10.1029/2006RG000207

Ruddiman WF, Raymo ME (2003) A methane-based time scale for Vostok ice. Quat Sci Rev 22:141–155

Ruddiman WF, Thomson JS (2001) The case for human causes of increased atmospheric CH_4. Quat Sci Rev 20:1769–1777

Ruddiman WF, Guo ZT, Zhou X, Wu HB, Yu YY (2008) Early rice farming and anomalous methane trends. Quat Sci Rev 27:1291–1295

Schmidt GA, Shindell DT, Harder S (2004) A note on the relationship between ice core methane concentrations and insolation. Geophys Res Lett 31:L23206. doi:10.1029/2004GL021083

Seltzer G, Rodbell D, Burns S (2000) Isotopic evidence for late Quaternary climatic change in tropical South America. Geology 28:35–38

Sepulcre S, Vidal L, Tachikawa K, Rostek F, Bard E (2011) Sea-surface salinity variations in the northern Caribbean Sea across the Mid-Pleistocene Transition. Clim Past 7(1):75–90. doi:10.5194/cp-7-75-2011

Singarayer JS, Valdes PJ, Friedlingstein P, Nelson S, Beerling DJ (2011) Late Holocene methane rise caused by orbitally controlled increase in tropical sources. Nature 470:82–85

Souma K, Wang YQ (2010) A comparison between the effects of snow albedo and infiltration of melting water of Eurasian snow on East Asian summer monsoon rainfall. J Geophys Res Atmos 115:D02115. doi:10.1029/2009JD012189

Spahni R, Chappellaz J, Stocker TF, Loulergue L, Hausammann G, Kawamura K, Fluckiger J, Schwander J, Raynaud D, Masson-Delmotte V, Jouzel J (2005) Atmospheric methane and nitrous oxide of the late Pleistocene from Antarctic ice cores. Science 310:1317–1321

Trenberth KE, Dai A, Rasmussen RM, Parsons DB (2003) The changing character of precipitation. Bull Am Meteorol Soc 84(9):1205–1217. doi:10.1175/BAMS-84-9-1205

Vandenberghe J (2000) A global perspective of the European chronostratigraphy for the past 650 ka. Quat Sci Rev 19(17–18):1701–1707

Vautard R, Yiou P, Ghil M (1992) Singular-spectrum analysis: a toolkit for short, noisy chaitic signals. Phys D 58:95–126

Verschuren D, Damste JSS, Moernaut J, Kristen I, Blaauw M, Fagot M, Haug GH, Members CP (2009) Half-precessional dynamics of monsoon rainfall near the East African Equator. Nature 462:637–641

Wadham JL, Tranter M, Tulaczyk S, Sharp M (2008) Subglacial methanogenesis: a potential climatic amplifier? Glob Biogeochem Cycles 22:GB2021. doi:10.1029/2007GB002951

Wahlen M (1993) The global methane cycle. Annu Rev Earth Planet Sci 21:407–426

Walter BP, Heimann M (2000) A process-based, climate-sensitive model to derive methane emissions from natural wetlands: application to five wetland sites, sensitivity to model parameters, and climate. Glob Biogeochem Cycles 14:745–765

Wang B (2006) The Asian monsoon. Springer, Berlin, p 787

Wang PX (2009) Global monsoon in a geological perspective. Chin Sci Bull 54:1113–1136

Wang B, Ding QH (2008) Global monsoon: dominant mode of annual variation in the tropics. Dyn Atmos Oceans 44:165–183

Wang PX, Tian J, Cheng XR, Liu CL, Xu J (2003) Carbon reservoir changes preceded major ice-sheet expansion at the mid-Brunhes event. Geology 31(3):239–242

Wang XF, Auler AS, Edwards RL, Cheng H, Cristalli PS, Smart PL, Richards DA, Shen CC (2004) Wet periods in northeastern Brazil over the past 210 kyr linked to distant climate anomalies. Nature 432:740–743

Wang PX, Clemens S, Beaufort L, Braconnot P, Dickens GR, Huber M, Jian ZM, Kershaw P, Sarnthein M (2005) Evolution and variability of the Asian monsoon system: state of the art and outstanding issues. Quat Sci Rev 24:595–629

Wang Y, Cheng H, Edwards RL, Kong X, Shao X, Chen S, Wu J, Jiang X, Wang X, An Z (2008) Millennial- and orbital-scale changes in the East Asian monsoon over the past 224,000 years. Nature 451:1090–1093

Winckler G, Anderson RF, Fleisher MQ, Mcgee D, Mahowald N (2008) Covariant glacial-interglacial dust fluxes in the equatorial Pacific and Antarctica. Science 320:93–96

Wolff E (2011) Global change: methane and monsoons. Nature 470(7332):49–50

Wolff E, Spahni R (2007) Methane and nitrous oxide in the ice core record. Phil Trans R Soc A 365:1775–1792

Wyrwoll KH, Miller GH (2001) Initiation of the Australian summer monsoon 14,000 years ago. Quat Int 83–85:119–128

Wyrwoll KH, Valdes P (2003) Insolation forcing of the Australian monsoon as controls of Pleistocene mega-lake events. Geophys Res Lett 30:2279. doi:10.1029/2003GL018486

Yasunari T (2007) Role of land-atmosphere interaction on Asian monsoon climate. J Meteorol Soc Jpn 85B:55–75

Yin QZ, Guo ZT (2006) Mid-Pleistocene vermiculated red soils in southern China as an indication of unusually strengthened East Asian monsoon. Chin Sci Bull 51:213–220

Yuan D, Cheng H, Lawrence Edwards R, Dykoski CA, Kelly MJ, Zhang M, Qing J, Lin Y, Wang Y, Wu J, Dorale JA, An Z, Cai Y (2004) Timing, duration, and transitions of the last interglacial Asian monsoon. Science 304:575–578

Zagwijn W (1996) The cromerian complex stage of the Netherlands and correlation with other areas in Europe. In: Tunrner C (ed) The early Middle Pleistocene in Europe. Balkema, Rotterdam, pp 145–172

Zheng Z, Lei ZQ (1999) A 400,000 year record of vegetational and climatic changes from a volcanic basin, Leizhou Peninsula, southern China. Palaeogeogra Palaeoecol Palaeocl 145:339–362

Ziegler M, Lourens LJ, Tuenter E, Reichart GJ (2010) High Arabian Sea productivity conditions during MIS 13—odd monsoon event or intensified overturning circulation at the end of the Mid-Pleistocene transition? Clim Past 6(1):63–76. doi:10.5194/cp-6-63-2010